PERSPECTIVE

Check for updates

Recent advances in porous organic cages for energy applications

Chao Liu, [ID] [a] Zhixuan Wang,[a] Hailong Wang [ID] *[b] and Jianzhuang Jiang [ID] *[b]

In recent years, the energy and environmental crises have attracted more and more attention. It is very important to develop new materials and technologies for energy storage and conversion. In particular, it is crucial to develop carriers that store energy or promote mass and electron transport. Emerging porous organic cages (POCs) are very suitable for this purpose because they have inherent advantages including structural designability, porosity, multifunction and post-synthetic modification. POC-based materials, such as pristine POCs, POC composites and POC derivatives also exhibit excellent energy-related properties. This latest perspective provides an overview of the progress of POC-based materials in energy storage and conversion applications, including photocatalysis, electrocatalysis (CO_2RR, NO_3RR, ORR, HER and OER), separation (gas separation and liquid separation), batteries (lithium–sulfur, lithium-ion and perovskite solar batteries) and proton conductivity, highlighting the unique advantages of POC-based materials in various forms. Finally, we summarize the current advances, challenges and further perspectives of POC-based materials in energy applications. This perspective will promote the design and synthesis of next-generation POC-based materials for energy applications.

[a]State Key Laboratory of New Pharmaceutical Preparations and Excipients, College of Chemistry and Materials Science, Hebei University, Baoding 071002, China

[b]Beijing Advanced Innovation Center for Materials Genome Engineering, Beijing Key Laboratory for Science and Application of Functional Molecular and Crystalline Materials, Department of Chemistry, School of Chemistry and Biological Engineering, University of Science and Technology Beijing, Beijing 100083, China. E-mail: hlwang@ustb.edu.cn; jianzhuang@ustb.edu.cn

1 Introduction

In order to achieve the goal of sustainable energy development, exploring and innovating renewable energy sources is critical to reducing the current serious dependence on fossil fuels. However, the region limitations of renewable energy such as tidal energy and solar energy are still a serious bottleneck for its large-scale practical application.[1] In addition, some energy-intensive industries have also urgently prompted researchers to develop advanced and sustainable energy-related technologies towards separation, rechargeable batteries, electrocatalysis and photocatalysis.[2] In order to further realize these advanced applications, it is imperative to develop novel materials with appropriate structures and functions. Recently, emerging materials based on porous organic cages (POCs), including pristine POCs, POC composites and POC derivatives, have attracted great attention due to their significant advantages compared to traditional inorganic materials in energy applications.[3–5]

Chao Liu was born in Hebei, China. He received his MSc (2012) and PhD (2022) degrees from the University of Science and Technology Beijing under the supervision of Prof. Dr Jianzhuang Jiang. Now, he works at Hebei University, and his research interest focuses on both porous organic cages and covalent organic frameworks.

Chao Liu

Zhixuan Wang was born in Hebei, China. She received her BSc (2023) degree from Xingtai University. Now, her research focuses on porous organic cages and photocatalysis under the supervision of Dr Chao Liu.

Zhixuan Wang

POCs, which are defined as porous organic compounds with cage-like structures, are usually self-assembled by two or more different structural organic units through covalent bonds. This makes the original POCs show the advantages of high porosity, diverse structures, rich functionality and easy tailorability. At the same time, the parent POCs can be adjusted by the post-modification strategy to further broaden their application range. POCs can be combined with other auxiliary components as functional carriers to create POC composites with predictable structures for a variety of applications. There are many cases in which ultrafine and stable metal nanoparticles (MNPs) are encapsulated by POCs.[6–8] In comparison with reticular frameworks such as covalent organic frameworks (COFs), metal–organic frameworks (MOFs) and hydrogen-bonded organic frameworks (HOFs),[9–14] the extended networks of POCs are composed of discrete porous molecules stacked by van der Waals forces, and their porous structures contain intercrossed molecule inner and external pores. POCs are able to be classified as supramolecular organic frameworks, being well characterized by mass spectrometry, nuclear magnetic spectroscopy, single crystal X-ray diffraction techniques, *etc.* The good solubility of POCs in solvents also makes it easy to process them into devices. On the other hand, POCs obtained by using irreversible bonds can be used as reaction precursors to derive different types of materials, such as COFs, MOFs, HOFs, *etc.*[15–20] POC derivatives have more exposed active sites and higher specific surface areas while retaining the functional advantages of POCs, which further improves their performances.

Although the fascinating structures and various novel applications of POC-based materials have attracted the in-depth exploration of researchers, and the applications of POC-based materials in the energy field have also been widely reported, there are still challenges in their practical applications. For example, due to the low sun light energy utilization of POC-based materials in photocatalysis and the low conductivity of electrocatalysis, it is still difficult to meet the actual industrial needs. In this perspective, we summarize the recent advances in the applications of POC-based materials in various energy-related fields. First, we introduce the special structural advantages of POC-based materials, and then comprehensively evaluate their applications in a wide range of energy technologies, including photo/electrocatalysis, separation, batteries and proton conductivity. We list the latest breakthroughs in the design, synthesis and application of POC-based materials. We hope that this perspective can summarize the latest and most effective information to help researchers understand and master the design strategies of POC-based materials more comprehensively. This is also true for the advantages and challenges when POCs are applied in different energy scenarios, helpful in increasing their economic value and broadening their application fields.

2 Porous organic cages (POCs)

2.1 Pristine POCs

As a new class of crystalline porous molecular-based materials, POCs are assembled from cage-like molecules formed by connecting different organic precursors by covalent bonds.[21–23] Because of the diversity of organic precursors, three-dimensional (3D) organic cage molecules have a variety of

Hailong Wang was born in Jilin, China. He received his BSc (2007), MSc (2010) and PhD (2013) degrees from Northeast Normal University, Shangdong University and the University of Science and Technology Beijing (USTB), respectively, under the supervision of Prof. Jianzhuang Jiang. During 2013–2018, as a postdoctoral fellow, he worked with Prof. Banglin Chen at the University of Texas at San Antonio and Prof. Qiang Xu at

Hailong Wang

the National Institute of Advanced Industrial Science and Technology. Now, he works at the USTB, focusing on porous molecule-based crystals and tetrapyrrole-based crystalline materials.

Jianzhuang Jiang was born in Heilongjiang, China. He received his BSc (1985), MSc (1988) and PhD (1993) (with Tsinglien Chang) degrees from Peking University. During his doctoral study (1990–1992), he obtained a fellowship from the Ministry of Culture, Science, and Sport of Japan and carried out his PhD work at Osaka University under the guidance of Keni-chi Machida and Ginya Adachi.

Jianzhuang Jiang

He was a Postdoctoral Fellow at Peking University with Tsinglien Chang (1993–1994), a Visiting Scholar at The Chinese University of Hong Kong with Dennis. K. P. Ng and Thomas C. W. Mak (1995–1996), and a Postdoctoral Fellow at the Queensland University of Technology with Dennis P. Arnold (1998–2000). He joined Shandong University and the University of Science and Technology Beijing in 1996 and 2008, respectively. He has been working on porphyrin- and phthalocyanine-based materials for more than thirty years to develop new single-molecule magnets, organic field-effect transistors, optical materials, energy materials and porous materials.

topological structures due to the incorporation of two or three components. Herein, the bicomponent topology is constructed by the number (m, n) of two organic building blocks, leading to $[m + n]$ topology. The adjacent cage molecules are stacked together to form cage exterior-pores, which are connected with the cavity inside the cage to form 3D intercrossing channels throughout the materials. The characteristics of organic precursors (such as bond angle, length, geometry, *etc.*) play a key role in adjusting the structures and functions of POCs, so that POCs have the advantage of more structural tunability than traditional porous inorganic materials. On one hand, the flexible integration of a wide range of selectable functional organic connectors enables POCs to be precisely designed for targeted applications such as catalysis, adsorption and separation.[24-27] On the other hand, the original POCs have well-defined pores and large specific surface areas. Combined with the weak forces provided by the specific groups attached on POCs, POCs can be used as special containers to encapsulate diverse guest species (molecules, clusters, nanoparticles, *etc.*), or POCs can be directly used as nanoreactors to achieve functional properties.[28-31] The unique properties of POCs combine readily available structures to further obtain performance–structure relationships to guide the rational design of POC based materials for energy applications.

So far, the vast majority of POCs are mainly obtained by the reactions involved in dynamic covalent chemistry (DvCC), such as imine condensation, boric acid ester condensation, and olefin/alkyne metathesis,[32-38] as shown in Table 1. The most thermodynamically stable molecular structure is fabricated by using the natural 'proof reading' and 'error checking' mechanisms due to the highly reversible covalent bonds. Usually, the synthesis process is simple, and the yield is high. Among the DvCC reactions, the imine condensation reaction is one of the most commonly used methods to synthesize well-defined POCs by selecting the appropriate preparation conditions. The reaction conditions include monomer concentration, reaction solvent type, catalyst and temperature. It is worth noting that

reversible reactions are not a necessary prerequisite for constructing POCs. In 2023, the Yuan group synthesized new stable [2 + 3] type sp² conjugated C=C bond-linked POCs by the Knoevenagel condensation reaction of bowl-shaped trialdehyde with two V type diacetonitriles, which provided more reaction ideas for constructing POCs.[39] POCs can be also connected by irreversible bonds, including C–C bonds, amide bonds, azide–alkyne cycloaddition and nucleophilic substitutions.[40-45] This type of chemical bond formation is rapid, and the obtained POCs have higher chemical stability. However, there are a large number of by-products, the yield is low, and the separation and purification are difficult. Therefore, there are relatively few reports on POCs based on these kinds of irreversible bonds. Importantly, in addition to considering their functionalities before designing POCs, the original POCs can be simply adjusted and designed by post-modification strategies such as modifying functional groups on the cage and inserting metal ions to generate/optimize specific functions. Therefore, the flexibility of POC structures makes them show great potential in various energy applications.

The crystallization process of POCs under controlled conditions is also very important. The Cooper group placed the desolvated organic cages in different organic solvent vapors (ethyl acetate, *o*-xylene, and dichloromethane), and obtained three non-porous, selective porous, and non-selective porous polymorphs, respectively.[46] The 'open' and 'close' of the micropores in POCs are realized by controlling conditions. In addition, the topological structure can be changed during the recrystallization of POCs. For example, the [3 + 6] triangular prism organic cage obtained by the reaction of tetraaldehyde and diamine can be transformed into a [6 + 12] tetrahedral organic cage after crystallization in dichloromethane and methanol.[47] Furthermore, the individual cages form interlocking organic cages during the crystallization process through the cleavage and reorganization of reversible bonds.[48]

POCs not only have porosity in the crystalline state, but also in the amorphous state. Common strategies for obtaining

Table 1 A summary of the bond forming reaction of POCs

Ligand 1	Ligand 2	Formed bond	Reaction type	Ref.
–CHO	–NH₂	–CH=N–	Imine condensation[a]	32
–B(OH)₂	–OH	–BO₂–	Boronic ester condensation[a]	38
–CHO	–CH₂CN	–CH=CC≡N–	Knoevenagel condensation[a]	39
–CHO	–C=ONHNH₂	–C=ONHN=CH–	Hydrazone condensation[a]	33
–SH	–SH	–S=S–	Disulfide bond exchange[a]	34
–C≡CR	–C≡CR	–C≡C–	Alkyne metathesis[a]	35
–C≡CR	–C≡CR	–C=C–	Olefin metathesis[a]	37
–C≡C	–N₃	(triazole structure)	Azide–alkyne cycloaddition[b]	40
–OH	–Cl/Br/I	–O–	Nucleophilic substitution[b]	41
–C≡CH	–C≡CH	–C≡C–C≡C–	Carbon–carbon coupling[b]	42
–Cl/Br/I	(pyridine)	(pyridinium structure)	Nucleophilic substitution[b]	43

[a] Reversible reactions. [b] Irreversible reactions.

© 2024 The Author(s). Published by the Royal Society of Chemistry

amorphous cage materials include interrupting crystallization during processing.[49] The Cooper group used the freeze-drying method to obtain a nearly double increase in Brunauer–Emmett–Teller (BET) surface area of amorphous solids, which is due to the increase in external pores available in disordered solids. Nevertheless, covalent interference reactions can also be used to hinder the crystallization of POCs.[50] By using different vertex diamines (ethylenediamine and cyclohexanediamine) to form a series of POCs with different vertices, the Cooper group obtained disordered stacking solids with a BET surface area of up to 818 $m^2 g^{-1}$.
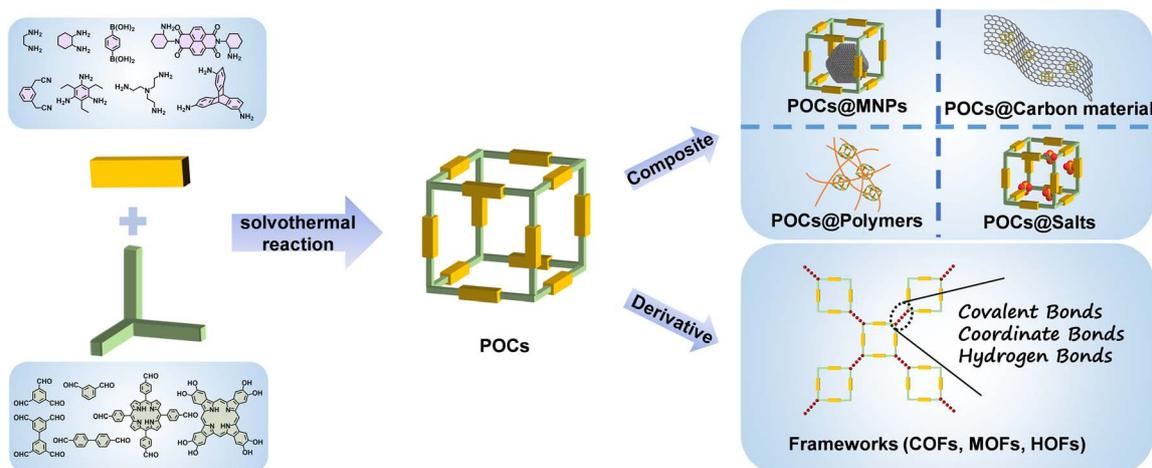
2.2 POC composites

With the increasing demand for efficient energy storage and conversion devices, it is sometimes difficult for these single-component materials to achieve better performance. Therefore, by combining POCs with various materials (carbon materials, polymers, MNPs, inorganic salts, *etc.*), the functionalities of POCs are further expanded to obtain a new generation of materials with improved performance. POC composites are a new type of material that combines POCs with other auxiliary materials. It can incorporate the advantages of two different materials and expand the functionalities of POCs through the synergy of the two species. In principle, POC-based composites can generally be divided into two categories according to the main functional components. For the first type of composite, POCs play a major role, and the auxiliary components will not directly participate in energy storage and conversion applications, but simply adjust the related properties of POCs. As an example, the combination of POCs and carbon materials in electrocatalysis improves the conductivity of the material, which makes POCs exhibit higher electrocatalytic performances. In the other type of composite, both POCs and auxiliary components play a key role in energy conversion and storage applications. The combination of POCs and MNPs is the most reported.[6–8] In this type of composite, POCs can be used as a new kind of host template to encapsulate and prepare ultrafine MNPs. The metal anchoring sites in the cage cavity can induce metal ion binding, nucleation and further growth of fine nanoparticles in the cage. The cage itself also acts as a protective shell for the generated MNPs to prevent their aggregation. In this direction, the tubular POC, MTC1, was prepared by the condensation of benzo[*c*][1,2,5]thiadiazole derivatives with cyclohexanediamine.[51] Ultrafine and well dispersed PdNPs (1.9 ± 0.4 nm) were prepared by using the interaction between nitrogen-containing sites and palladium ions in MTC1. The synergistic effect of PdNPs and the photocatalyticactive POC in Pd@MTC1 composites achieved a two-step sequential reaction from 4-nitrophenylboronic acid to 4-aminophenol. So far, gold, silver, palladium, ruthenium, rhodium, platinum, iridium and other precious MNPs based on POCs have been reported, which are widely used in thermal catalysis and photocatalysis.

2.3 POC-derived materials

POCs are also used as precursors to construct other forms of materials through a variety of ways, and cage-to-framework strategies have been studied for higher performance applications. Generally, the preparation of POC derivatives is mainly based on the post-synthetic modification strategy of the original POCs. In essence, most POCs have low conductivity and poor stability under extreme environmental conditions, in particular for photo/electrocatalytic reactions in strongly acidic or alkaline electrolytes. The good dissolution of POCs in some organic solvents limits their heterogeneous applications, hindering their practical applications to a certain extent. Fortunately, the original POCs can be directly used as special building blocks to derive various materials, including COFs, MOFs and HOFs (Scheme 1). The POC derivation method is an effective synthesis strategy to expand and optimize their functions. In particular, compared to the weak van der Waals force between POC molecules, the covalent bonds, coordination bonds and hydrogen bonds endow the derived materials with stronger stability. The obtained POC derivatives not only inherit the structural advantages of the original POCs, but also further improve their carrier mobility and specific surface area. The uniform dispersion of the active centers in the POC building

Scheme 1 Schematic illustration of pristine POCs, POC composites and POC derivatives.

blocks in the derivatives exposes more active sites and improves the utilization of intrinsic active sites, which leads to impressive performance in energy applications, including adsorption separation and catalysis. Recently, the Chen group prepared cage-based MOFs (mcm-MOF-1) by using a 6-connected [2 + 3] trigonal prismatic cage and Cu^{2+}. Mcm-MOF-1 has high specific surface area and can adsorb aniline efficiently in the liquid phase.[15] A porous HOF was prepared based on non-porous organic cages. The specific surface area of HOF material obtained by cage transformation is as high as 685 m^2 g^{-1}, and an efficient catalytic Suzuki reaction was achieved after loading divalent Pd ions.[52]

Not only can the POCs be used as a building block directly, but they also can be converted into other materials by DvCC-induced dissociation and reconstruction. The converted materials often retain some of the characteristics of the parent POCs. The Hou group used chiral POCs to obtain COF materials without chiral groups through joint exchange, but COFs can retain the chiral information of the original organic cage, and the prepared materials show excellent chiral separation performance.[53] There is another example where the materials prepared by the cage-to-COF conversion strategy have a higher specific surface area. In 2020, for the first time, the Zhang group realized the transfer of POCs to COFs through DvCC.[54] Later, the Patra group transformed POC molecules into 2D COF films with higher crystallinity and specific surface area through DvCC at room temperature.[55] The film can be used for size-selective molecular separation. In the same year, the COFs prepared based on POCs showed a higher specific surface area and iodine adsorption capacity than the directly synthesized COFs.[56]

3 The energy applications of POCs

The rapid consumption of non-renewable fossil fuels has caused a serious energy crisis and environmental problems. Newly developed POC-based materials are used to deal with these problems. In the past decade, topological design and functional unit synthesis strategies have been rapidly developed as two basic aspects of the POC field, greatly supplementing molecular design and functional exploration. Thus far, in the process of constructing functional POCs, the most common strategy is to design and develop corresponding POC materials based on specific functional units. In addition, functional optimization can also be achieved by combining POCs with other materials (MNPs, organic polymers, carbon materials, salts, *etc.*) or constructing other types of derivatives based on POCs. Using POCs to synthesize POC-derived materials is also an optional strategy to obtain higher performance materials. The energy applications of POC-based materials mainly focus on photocatalysis, electrocatalysis, separation, batteries and proton conductivity.

3.1 Photocatalysts

3.1.1 POCs as photocatalysts. Visible light photocatalysis has always been a research hotspot in the field of chemistry and the environment due to its mild reaction conditions and

abundant solar energy. Up to now, there are several cases in which POCs have been directly used as photocatalysts. The research on POCs started very late, and current research on POC photocatalysis is still limited. At the same time, the absorption of visible light by the materials is crucial in the photocatalytic process, and most organic building blocks have weak or no absorption of visible light, which limits the development of their performances. Based on the flexibility of POC molecular structure design, the general strategy is to introduce active light absorption chromophores to improve visible light photocatalytic performance. Porphyrins are a class of macromolecular heterocyclic compounds formed by the covalent interconnection of four pyrroles. Their high degree of conjugation endows them with strong visible light capture ability, which is often used for visible light photocatalysis. Based on these characteristics, multiple porphyrin-based organic cages were designed for visible light photocatalysis (Fig. 1). In 2018, the Kim group designed a [6 + 8] type porous porphyrin box (Zn-PB) composed of 6 square zinc porphyrin units and 8 triangular units.[57] The unique photochemical behavior of the triplet excited state of porphyrin compounds, combined with the porous structure of the material, allows Zn-PB to efficiently produce singlet oxygen under visible light. Later, this group also designed the largest porphyrin organic cage (*ca.* 5.3 nm) so far,[58] $P_{12}L_{24}$, built with 12 square-shaped porphyrins and 24 bent linkers. Since the large pores of $P_{12}L_{24}$ facilitate the diffusion of substrate molecules, $P_{12}L_{24}$ effectively catalyzes the photooxidation of dihydroxynaphthalene derivatives in a heterogeneous environment. $P_{12}L_{24}$ also shows an obvious size effect in photocatalysis. When the size of the catalytic substrate is large, the catalytic conversion rate of $P_{12}L_{24}$ is significantly higher than that of other small-sized porphyrin organic cages.

Another example of a porphyrin organic cage for visible light photocatalysis was reported in 2020.[59] The [3 + 6] tubular organic cage, PTC-1(2H), is composed of three porphyrin segments and six diaminocyclohexane groups linked by 12 imine bonds. The long triplet lifetime and microporous supramolecular framework of PTC-1(2H) ensure high-efficiency singlet oxygen evolution. Based on this, PTC-1(2H) can realize heterogeneous visible light photocatalysis of various primary
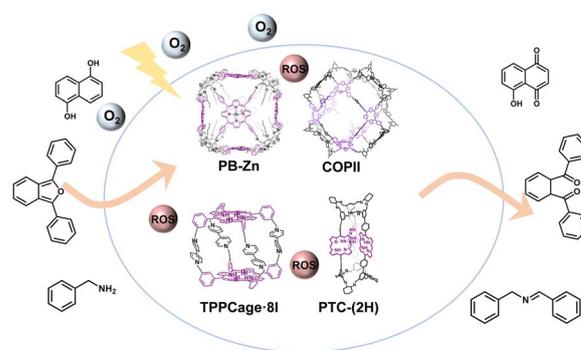

Fig. 1 Porphyrin-based POCs with different topological structures generate reactive oxygen species (ROS) under visible light for multiple photocatalytic organic conversion reactions.

amines, and the conversion rate is more than 99%. Its photocatalytic efficiency exceeds that of the typical mesoporous MOF material, PCN-222. In addition to porphyrin as a photoactive group, POCs based on conjugated groups such as pyrene[60] and thiazole[61,62] also exhibit high photocatalytic activity.

The structure modification of POCs is also an effective method to improve their photocatalytic performances. To date, ionization of POCs is an effective means to improve their photocatalytic performance. In 2022, the Chang group attempted to introduce additional second-sphere functionalities into the organic cage supramolecular framework, and the synergy between multiple interactions improves the photocatalytic activity (Fig. 2a–c).[63] Based on the previously reported topological structure of Zn-PB, an alkynyl-functionalized porphyrin box (FePB-3(N)) was designed, and then 24 positively charged ammonium groups were added to the organic cage molecule by a synthetic post-modification strategy to obtain FePB-2(P). The synergistic effect of porosity and charge enhances the photocatalytic CO_2RR performance. Through the comparison in a series of experiments, the CO_2RR photocatalytic activity of the bifunctional FePB-2(P) is more than 40 times higher than that of the FeTPP reference materials. In contrast, CO_2RR photocatalytic activity of materials with only pores or only charge interactions are increased by 4 times or 6 times, respectively. The selectivity of FePB-2(P) for photocatalytic reduction of CO_2 to CO is 97%, and its turnover frequency (TON) is more than 1100. Similarly, the Sun group designed another porphyrin cage, TPPCage·8I.[65] This ionization strategy effectively avoids the spontaneous aggregation of porphyrins by utilizing the naturally occurring electrostatic repulsion between adjacent cage hosts. At the same time, hydrophilic iodine ions also provide additional heavy atom effects. These modifications significantly enhance the photophysical properties and lead to

extraordinary catalytic activity in the photocatalytic oxidative coupling reaction of benzylamine.

The optimization of photocatalytic performance is achieved by regulating the metal ions of N_4 coordination in the porphyrin center. In 2022, the Li group used 5,10,15,20-tetrakis(4-hydroxyphenyl)porphyrin as the surface and 2,4-dichloro-6-phenyl-1,3,5-triazine as the pillar to prepare a metal-free porphyrin organic cage, P@POC, by a stepwise nucleophilic substitution reaction (Fig. 2d–g).[64] Then, by refluxing the mixture of P@POC and $CoCl_2$ or $ZnCl_2$, a single Co or Zn atom is embedded in the porphyrin ring by a post-synthetic modification strategy. The introduction of metal ions into the N_4 cavity of porphyrin significantly improves the light absorption and promotes the separation and transfer of photogenerated electrons. The Co atom-anchored organic cage (CoP@POC) has a more prominent photocatalytic efficiency in oxidizing amines into imines under visible light. The reaction conversion and selectivity of CoP@POC are as high as 99%, and the TOF is 1389 h^{-1}, superior to those of most reported photocatalysts.

3.1.2 POC-based composites as photocatalysts. In addition to the organic cage itself as a photocatalyst, the cavity inside the molecule makes it suitable as a molecular container to accommodate other materials, and the obtained composites have ultra-high photocatalytic activity. The most common is the combination of organic cages and noble MNPs. The Mukherjee group reported a triangular prismatic organic cage (OC1^R) synthesized by self-assembly imine condensation of phenothiazine trialdehyde and chiral 1,2-cyclohexanediamine building blocks.[66] This newly designed cage has an aromatic wall and a porous interior. Two cyclic sulfides and three adjacent diamines are suitable for binding gold ions, which can be used to design ultrafine and stable AuNPs. The AuNPs with a narrow size distribution were synthesized by encapsulating and reducing Au^{3+} in a functionalized cage. The Au content of the
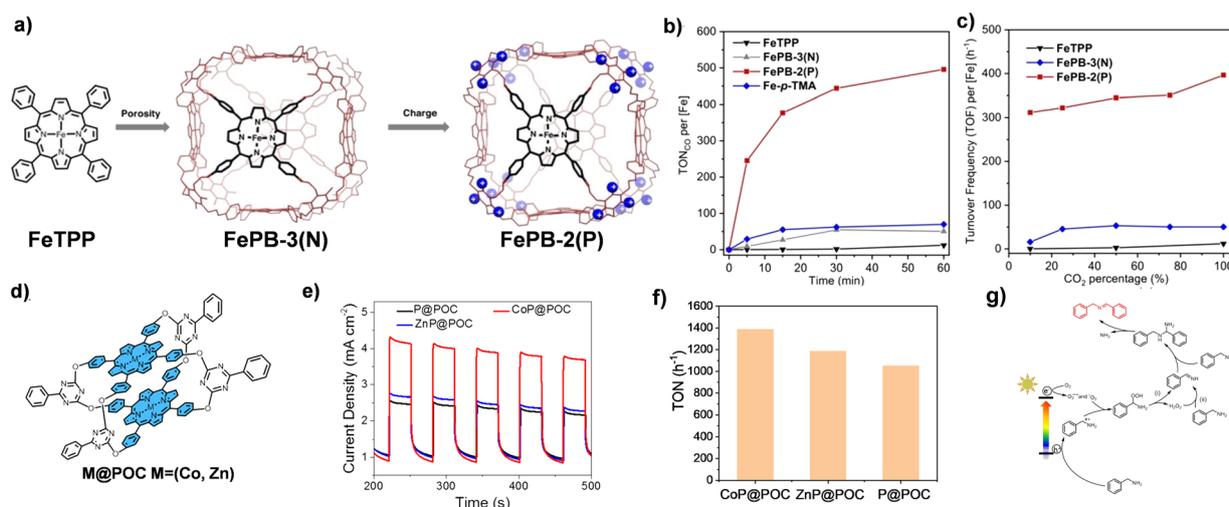
Fig. 2 (a) The design of FePB-3(N) and FePB-3(P) catalysts; (b) photocatalytic CO_2RR activity of FePB-2(P), FePB-3(N), FeTPP and Fe-p-TMA in CO_2-saturated DMF; (c) photochemical CO_2RR activity of FePB-2(P), FePB-3(N) and FeTPP in DMF at different CO_2 concentrations. Reproduced from ref. 63. Copyright 2022, Wiley-VCH. (d) The molecular structures of P@POC and M@POC; (e) photocurrent response of P@POC, CoP@POC and ZnP@POC; (f) comparison of photocatalytic activity of P@POC, CoP@POC and ZnP@POC; (g) photocatalytic mechanism of oxidative coupling of benzylamines. Reproduced from ref. 64. Copyright 2022, The American Chemical Society.

composite Au@OC1^R is as high as 68 wt%. In the absence of cage encapsulation, direct reduction of gold salts will produce unstructured aggregates. Au@OC1^R is used as a potential heterogeneous photocatalyst for the conversion of nitro-aromatics to the corresponding azo compounds in only 2 h at ambient temperature. This material has excellent chemical stability and reusability, and no AuNP agglomeration occurs even after the 5th catalytic cycle. The composite Au@OC1^R represents the first example of organic cage-loaded AuNPs as photocatalysts. Similarly, the Dong group reports a new composite material of Ag NPs loaded with POCs (CC3-OH), Ag@CC3-OH.[67] As a highly efficient heterogeneous catalyst, Ag@CC3-OH can also selectively photoreduce nitroaromatics to azo compounds under visible light irradiation with a conversion rate of up to 99%.

Later, a light-controlled active group is introduced into POCs to encapsulate NPs. In 2021, the Maji group designed a photo-chromic organic cage (TAE-DTE) based on a dithienylethene (DTE) unit (Fig. 3a–e).[68] Subsequently, stable ultra-small (<2 nm) AuNPs (Au@TAE-DTE) were prepared by a unique reverse double solvent method. Au@TAE-DTE exhibits photochromic properties similar to those of TAE-DTE. Based on the opening and closing of the DTE ring, two metastable photoisomers are transformed between Au@TAE-DTE-O and Au@TAE-DTE-C. The Au@TAE-DTE composite can realize the catalytic reduction of CO_2 under visible light (λ = 400–750 nm). In addition, Au@TAE-DTE-O and Au@TAE-DTE-C coexist under full-range (λ = 250–750 nm) light irradiation, showing wider spectral absorption and significantly enhanced photocatalytic CO_2 reduction performance. This case is based on the encapsulation of MNPs by light-controlled organic cages, which improves its catalytic activity and selectivity.

The composite material Ag^O@OB4^R represents the first example of discrete POC encapsulated Ag NPs, which were used as a photocatalyst in an Ullmann-type coupling reaction at room temperature (Fig. 3f–i).[69] A discrete tetragonal organic cage (OB4^R) is reported by the Mukherjee group, which is formed by the condensation of imine bonds between rigid tetraaldehyde
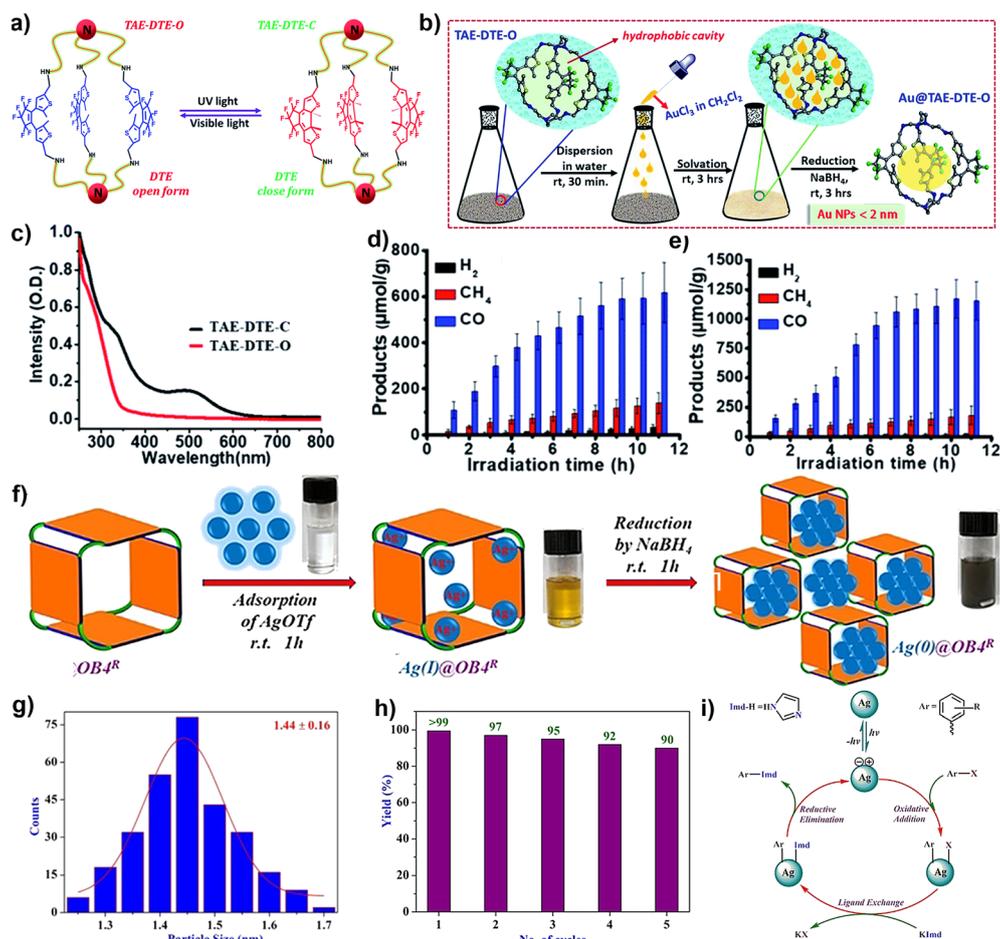
Fig. 3 (a) The molecular structures and structure interconversion of TEA–DTE–O and TEA–DTE–S; (b) the electronic absorption spectra of TEA–DTE–O and TEA–DTE–S; (c) schematic diagram for *in situ* growth and stabilization of Au NPs inside the organic cage; CO_2 reduction using Au@TAE-DTE-O under (d) visible light (400–750 nm) and (e) full-range light (250–750 nm). Reproduced from ref. 68. Copyright 2021, The Royal Society of Chemistry. (f) Pictorial representation of the formation of Ag(0)@OB4^R; (g) particle size distribution of Ag(0)@OB4^R; (h) reusability plot of Ag(0)@OB4^R; (i) reaction pathway for Ullmann-type aryl-amination coupling by using photocatalyst Ag(0)@OB4R. Reproduced from ref. 69. Copyright 2020, Wiley-VCH.

and flexible diamine, and then the reduction of imine bonds. $OB4^R$ can be used as a molecular container to control the nucleation of AgNPs, and the size can be finely adjusted by binding with Ag^+ in a closed cavity, and then reduced to obtain ultrafine AgNPs. The average particle size of $Ag^0@OB4^R$ was 1.44 $\pm$ 0.16 nm, and the silver content was about 52 wt%. With an efficient photocatalyst, the Ullmann-type arylamine coupling of halogenated aromatic hydrocarbons can be easily achieved at ambient temperature.

In addition to AuNPs and AgNPs, PdNPs also can be encapsulated in POCs. The Wei group reported a highly catalytically active nanocomposite based on PdNPs and POCs for the photoreduction of CO_2 to CH_4 in the presence of a photosensitizer, tris(2,2'-bipyridyl) ruthenium chloride(II).[70] The PdNPs with a diameter of 4.7 nm can achieve a high selectivity of 97% for CO_2 to CH_4 photoreduction at a rate of 10.2 μmol g^{-1} h^{-1}. When these PdNPs are co-assembled with POCs (CC3), the catalytic efficiency of CO_2 photoreduction is significantly enhanced (78.5 μmol g^{-1} h^{-1}), which is mainly due to the increase in CO_2 absorption by these cage compounds. In addition, the effect of the size of PdNPs on the photoreduction was also discussed. The smaller size of PdNPs leads to a higher reaction rate but lower selectivity, while the larger size of PdNPs results in a lower reaction rate but higher selectivity. These self-assembled nanocomposites also exhibit high CO_2 photoreduction performance under a low CO_2 atmosphere with an evolution rate of 34.5 μmol g^{-1} h^{-1}.

3.1.3   POC-derived materials as photocatalysts. The cage-to-framework strategy is also an effective method to improve POC photocatalytic performance. The organic cage is not only a molecular porous material, but it also can be used as a building block to prepare porous frameworks. The Kim group used the designed zinc porphyrin box, Zn-PB, as a node to react with suitable dipyridyl-terminated bridging ligands, constructing PB-based layered superstructures (PSSs).[57] The stable structure of PSS is not only derived from the coordination bond between Zn ions and bipyridine-terminated ligands, but also

the π–π interaction between the corners of the Zn-PB units, as shown in Fig. 4. Compared with the PB, PSS has a larger void volume and specific surface area. PSS-1 is more effective than its component Zn-PB in catalyzing the singlet oxygen-induced synthesis of the natural product walnut ketone, and its photocatalytic efficiency is greatly improved. At the end of this section, it is worth noting that in the practical photocatalytic application of some organic porous materials, the synergistic combination of functional units including porphyrin, nanoparticles and framework structures shows improved photocatalytic efficiency.[71–74] In future research, POC materials can be considered to master the synergistic effect of these three methods to enhance photocatalytic performance.

3.2   Electrocatalysis

POCs, POC-based composites and POC-derived materials play an important role in converting light energy into chemical energy. They are not only excellent in the field of photocatalysis, but also represent a kind of star material in the field of electrocatalysis, and have aroused strong research interest of scientists. The electrocatalytic applications of POC-based materials are mainly focused on the CO_2 reduction reaction (CO_2RR), oxygen reduction reaction (ORR), hydrogen evolution reaction (HER), nitrate reduction reaction (NO_3RR), oxygen evolution reaction (OER) and so on.

3.2.1 CO_2RR. The content of carbon dioxide in the atmosphere is increasing, leading to serious environmental problems, such as global warming, sea level rise and extreme weather. The research on photoreduction of carbon dioxide has made good progress. In addition, electrochemical carbon dioxide reduction is also a promising solution for energy conversion. It can not only convert carbon dioxide into key chemical raw materials and fuels under environmental conditions, but also realize the storage of renewable energy. The design and construction of highly active organic cage molecular-based electrocatalysts is crucial for the development of materials and supramolecular chemistry.

The chloroiron(III) porphyrin box (Fe-PB) was designed by reacting the previously reported porphyrin organic cage PB-1 with $FeBr_2$.[75] Compared with the monomer catalyst, the large cavity of PB-1 facilitates the exposure of active sites and substrate diffusion, thus generating carbon monoxide with a higher rate, Faraday efficiency, current density and TON in water at pH 7.3. Fe-PB did not significantly change the reaction mechanism compared with 1, indicating that the POC structure could enhance the electrocatalytic efficiency. These results provide a new idea for the design of supramolecular catalysts. It is also the first case of electrocatalytic reduction of carbon dioxide to carbon monoxide by POC molecular materials. In 2023, a series of cofacial porphyrin POCs (CPOC-M, M = H_2, Co(II), Ni(II), Cu(II) and Zn(II)) were constructed from 5,10,15,20-tetrakis(4-formylphenyl) porphyrin (TFPP) and chiral(2-aminocyclohexyl)-1,4,5,8-naphthalimide (ANDI) via covalent template self-assembly and subsequent metallization,[76] as shown in Fig. 5a–e. The photophysical behavior and electrocatalytic performance of CO_2 reduction were studied
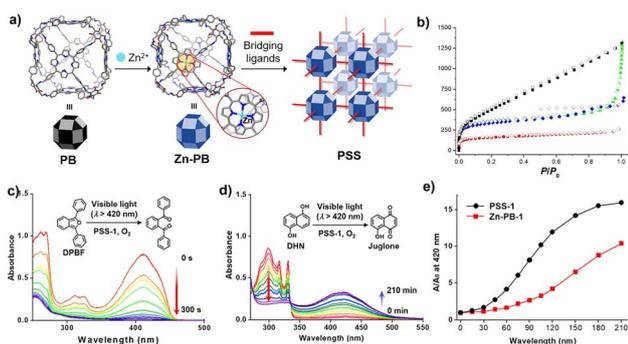
Fig. 4 (a) Construction of cage–based MOFs by using a porphyrin box; (b) N_2 sorption isotherm at 77 K for 'PB' (red), 'PSS1' (black), 'PSS3' (green) and 'PSS4' (blue); electronic absorption spectra of DPBF (c) and DHN (d) in the presence of PSS-1, O_2 and visible-light irradiation; (e) comparative catalytic performance of PSS-1 (black) and Zn-PB (red) for oxidation of DHN. Reproduced from ref. 57. Copyright 2018, The American Chemical Society.
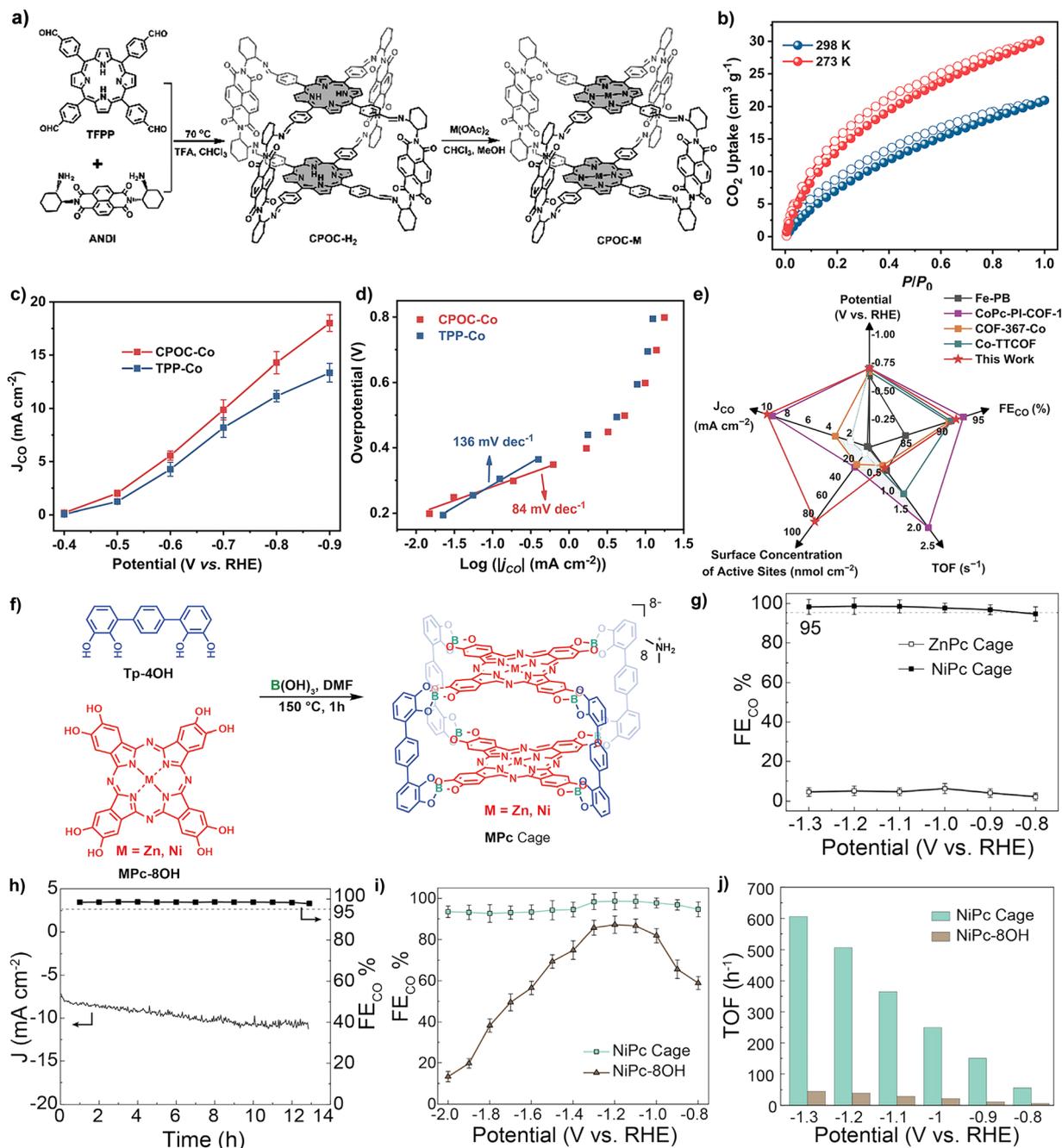
Fig. 5 (a) Schematic synthesis of CPOC-M (M = H$_2$, Co(II), Ni(II)); (b) CO$_2$ adsorption (solid) and desorption (hollow) curves of POC-H$_2$; (c) comparison of the partial CO current density between CPOC-Co and TPP-Co; (d) Tafel plots of CPOC-Co and TPP-Co; (e) comparison of the performance to that of other materials. Reproduced from ref. 76. Copyright 2023, The Royal Society of Chemistry. (f) Pictorial representation of the formation of an MPc cage; (g) CO faradaic efficiency of ZnPc and NiPc cages; (h) stability test of the NiPc cage at 1.2 V for 13 h; (i) CO faradaic efficiency of the NiPc cage and NiPc-8OH; (j) TOF comparison of the NiPc cage and NiPc-8OH. Reproduced from ref. 77. Copyright 2023, The Cell Press.

comprehensively. According to the results of femtosecond transient absorption spectroscopy, the photoexcitation of CPOC-H$_2$ and its subsequently synthesized Zn and Co counterparts leads to a rapid energy transfer from the triplet porphyrin to the NDI unit. In addition, compared with other metals CPOC-M (M = Ni(II), Cu(II), Zn(II)) and monomeric porphyrin cobalt, CPOC-Co has better electrocatalytic activity,

providing a partial current density of 18.0 mA cm^{-2} at −0.90 V, and the Faraday efficiency of CO is 90%.

Similar to the porphyrin molecular structure, planar conjugated macrocyclic phthalocyanine (Pc) is also an excellent electrocatalytic active group. Due to the large aromatic system and modifiable structure, it can act as a catalyst in the electrochemical reaction to achieve the CO$_2$ reduction reaction.

However, the synthetic challenges associated with geometric requirements and poor solubility of phthalocyanines lead to only one discrete shape-persistent POC composed of Pc parts. The Zhang group reported the synthesis of Zn and Ni metallized phthalocyanine molecular cages by one-step connection from dynamic borates, and revealed the cage-like structure of ZnPc by single crystal X-ray diffraction (Fig. 5f–j).[77] In addition, the isolated redox active metal sites, easily accessible cavities and stable skeletons ensure that nickel-metallized phthalocyanine (NiPc) cages exhibit high catalytic efficiency, selectivity and stability, and are superior to other molecules in the electrocatalytic CO_2RR.

The electrocatalytically active sites of the POCs described above are located in the cage. In addition, with the help of the cavity of POCs and the special adsorption capacity of CO_2, it can also be combined with other materials to improve its electrocatalytic performance. The Han group reported a strategy to enhance the electrocatalytic reduction of CO_2 to multi-carbon products by using CC3 as an additive to improve the diffusion of CO_2 to the Cu-nanorod catalyst surface.[78] In this work, nanocatalysts were combined with CC3 and used as catalysts in a gas-diffusion electrode. Studies have shown that the addition of CC3 can significantly improve the efficiency of various nanocatalysts (Fig. 6). Among them, the Faraday efficiency of the Cu-nanorod/CC3 composite catalyst can reach 76.1%, and the current density is 1.7 A cm^{-2}. Studies have shown that the pores of CC3 can absorb the CO_2 accumulated during the reaction, and the CO_2 in CC3 is easier to diffuse into the catalytic layer than the CO_2 in the liquid electrolyte. This work opens up a new way to design and construct an efficient CO_2RR catalyst.

3.2.2 NO_3RR, ORR, HER and OER. Thus far, only one electrocatalytic NO_3RR example has been reported. The Chang group tried to use the dual characteristics of supramolecular porosity and affinity for NO_3^- in the electrocatalytic NO_3RR. The
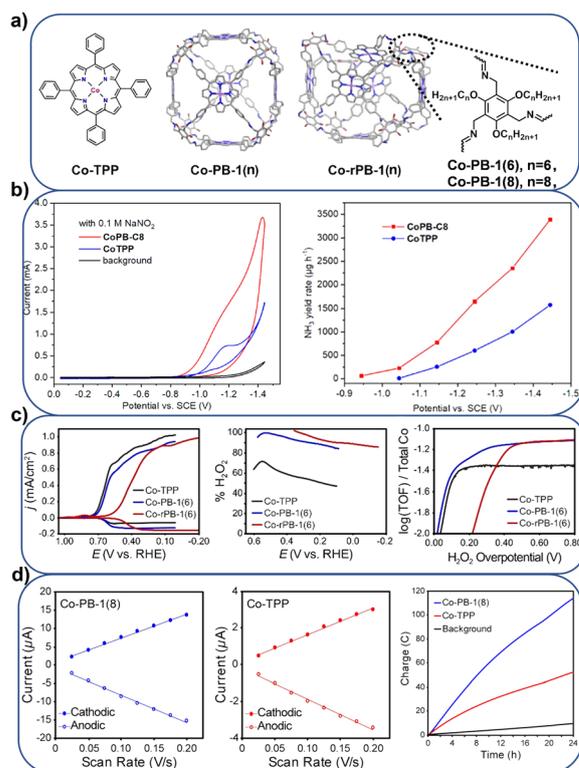

Fig. 7 (a) Pictorial representation of different porphyrin boxes; (b) the NO_3RR performance comparison of CoPB-1(8) and Co-TPP; Reproduced from ref. 79. Copyright 2023, Wiley-VCH. (c) The ORR performance comparison of Co-PB-1(6), Co-rPB-1(6) and Co-TPP; Reproduced from ref. 80. Copyright 2020, Wiley-VCH. (d) The HER performance comparison of Co-PB-1(8) and CoTPP. Reproduced from ref. 81. Copyright 2021, Wiley-VCH.

Chang group reported that the integration of two-dimensional (2D) molecular cobalt porphyrin (CoTPP) catalyst units into a three-dimensional (3D) POC (CoPB-1(8)) significantly improves its electrocatalytic activity and stability (Fig. 7a and b).[79] This supramolecular catalyst can promote efficient NO_3RR to produce ammonia with high selectivity (>90% Faraday efficiency), and the TON and TOF values are 200 000 and 56 s^{-1}, respectively. In contrast to CoTPP, the catalytic efficiency of CoPB-1(8) increased by 15 times, which can be attributed to the increase in electrochemically active cobalt centers and the supramolecular adsorption of NO_3^- on the CoPB-1(8) catalyst. Further modification of peripheral alkyl substituents reveals the important influence of cage porosity and cavity size on the electrochemical NO_3RR. This research group also assembled a permanently porous supramolecular cage Co-PB-1 for a selective ORR catalyst,[80] which contains 6 Co-TPP subunits and is connected by 24 imine bonds (Fig. 7a and c). These imine connectors were reduced to amines to obtain a more flexible cage-like Co-rPB-1. Co-PB-1 and Co-rPB-1 produced 90–100% H_2O_2 by the electrocatalytic ORR in neutral pH water, while the Co-TPP monomer produces a mixture of 50% H_2O_2 and H_2O. The high H_2O_2 selectivity is attributed to the site isolation of discrete molecular units in a supramolecular solid. The same
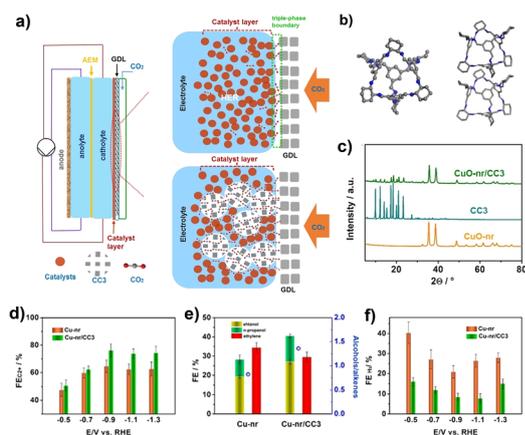

Fig. 6 (a) Schematic diagram of the flow-cell; (b) the crystal structure of CC3; (c) the XRD patterns of CC3, CuO-nr and CuO-nr/CC3; (d and e) the FE of C^{2+} products and H$_2$ at different potentials of Cu-nr/CC3 and Cu-nr; (f) FE of C^{2+} alcohols and ethylene over different catalysts at a potential of 0.9 V versus RHE. Reproduced from ref. 78. Copyright 2022, Wiley-VCH.
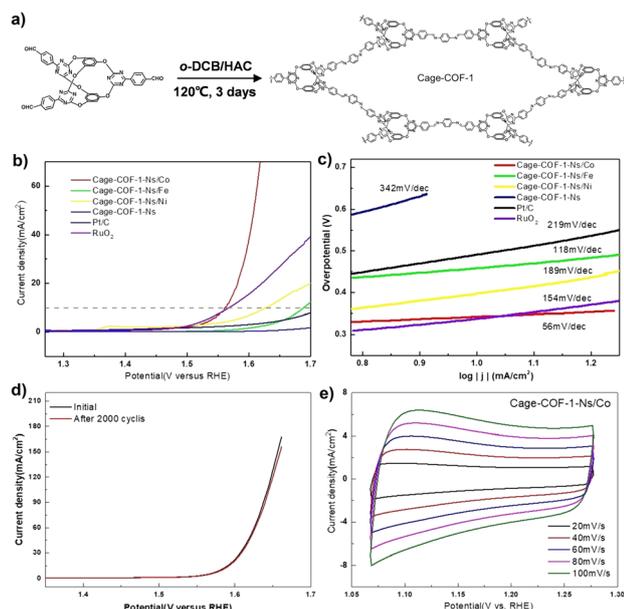
Fig. 8 (a) The synthesis and structure of a POC-derived material, Cage-COF-1; (b) OER polarization curves for different Cage-COF-1-Ns; (c) Tafel slopes of Cage-COF-1-Ns in the OER; (d) OER polarization curves of Cage-COF-1-Ns/Co before and after 2000 potential cycles; (e) the CV curves of Cage-COF-1-Ns/Co. Reproduced from ref. 82. Copyright 2022, Wiley-VCH.

material, Co-PB-1,[81] was used for the electrochemical HER (Fig. 7a and d). Compared with CoTPP, the electrochemically active cobalt atoms of the Co-PB-1 film are increased by five times. The Tafel slope of Co-PB-1 is 119 mV per decade, and the HER activity reached 19 000 turnovers with 100% Faraday efficiency in over 24 hours.

In addition, the cage-to-COF strategy has also been explored to develop high-performance electrocatalysts.[82] The Chen group used bicyclocalix[2]arene[2]triazines tri-aldehyde as a building block to design and synthesize POC derivatives, Cage-COF-1 (Fig. 8). The cage-like structure results in a weak interaction between adjacent layers in the COF structure, which can exfoliate the original bulk COF into thin COF nanosheets (Cage-COF-1-Ns). Subsequently, Cage-COF-1-Ns/Co was obtained by post-modification of Co^{2+}. The material has a low overpotential (330 mV) and Tafel slope (56 mV dec^{-1}) in the OER, showing good catalytic activity and stability.

So far, there are only limited electrocatalytic reactions based on the POC-based materials described above, and more types of electrocatalytic reactions still need to be further explored. These cases have shown the important role of POCs with discrete catalytically active sites in electrocatalytic reactions. The versatility of POCs as supramolecular platforms for the development of adjustable and efficient electrocatalysts will continue to be expanded.

3.3 Separation

3.3.1 Gas separation. Industrial separation is a challenging and energy-intensive technology. Adsorptive separation

becomes an alternative technology due to its low energy consumption. POCs have broad application prospects in gas separation due to their unique structures. In this section, we summarize the significant progress made by POCs in the separation of various industrial gases, such as light hydrocarbons, noble gases and D_2/H_2.

Light hydrocarbon (LH) separation is a key process in the petrochemical industry. At present, the separation is achieved mainly by low temperature distillation, which consumes a lot of energy in the separation process. The use of porous solids as adsorption and separation materials has received extensive attention due to its lower energy consumption and higher efficiency. POCs have excellent stability, an adjustable pore structure and abundant adsorption active sites, POCs can be used as a new type of adsorbent to separate light hydrocarbons. The Yuan group proposed a new strategy to adjust the gas adsorption and separation performance by using different supramolecular isomers of the same POC molecule.[83] A lantern-like calix[4]resorcinol calixarene-based POC, CPOC-101, was prepared, and eight different solvatomorphs can be obtained by crystallization in different solvents. Those solvatomorph materials show significant differences in gas adsorption capacity and separation ability. The Brunauer–Emmett–Teller (BET) surface area of CPOC-101α crystallized in toluene/chloroform was as high as 406 m^2 g^{-1} measured by nitrogen adsorption at 77 K, which was much higher than that of other CPOC-101 solvatomorphs. More interestingly, the C_2H_2 and CO_2 adsorption capacity of CPOC-101α and the C_2H_2/CO_2 separation selectivity at room temperature are superior to those of the representative of POC solvatomorphs. Later, two novel nitrogen-rich POCs, CPOC-107 and CPOC-203, were constructed from bowl-shaped tetraformylcalix[4]resorcinol calixarene and different nitrogen-rich imidazolyl diamines.[84] CPOC-107 has a [2 + 4] lantern-like structure, while CPOC-203 has a [3 + 6] triangular prism structure (Fig. 9). In addition, CPOC-107 has a large cavity volume of up to 787 $Å^3$ and a high BET specific surface area of up to 1202
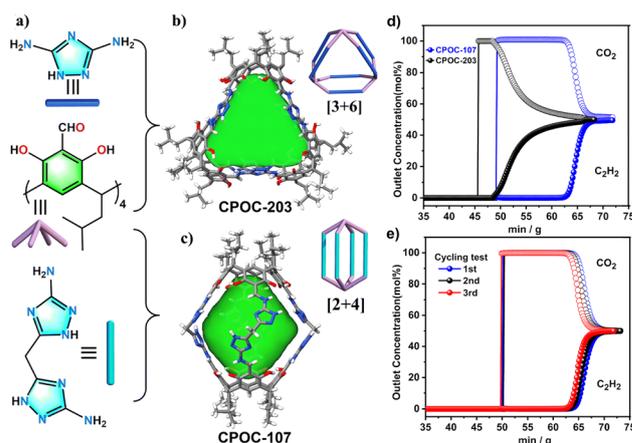

Fig. 9 (a–c) The chemical and crystal structures of CPOC-203 and CPOC-107; (d) experimental breakthrough curves for an equimolar mixture of C_2H_2/CO_2 at 298 K; (e) the recyclability of CPOC-107 under multiple mixed gas column breakthrough tests. Reproduced from ref. 84. Copyright 2023, The Royal Society of Chemistry.

$m^2 g^{-1}$. Their high specific surface area and high nitrogen content show that both cages showed good C_2H_2 adsorption capacity. Specifically, CPOC-107 achieved a C_2H_2 adsorption value of up to 146 $cm^3 g^{-1}$ at 298 K and 1 atm, which is the highest among all porous organic materials. The experimental breakthrough test confirms the effective separation of the C_2H_2/CO_2 mixture by the CPOC-107 adsorbent, and the breakthrough time is 13 min g^{-1}. This study suggests that nitrogen-rich POCs may be more promising materials for C_2H_2 storage and purification.

The Zhang group reported another flexible and stable POC crystal (NKPOC-1-α), which can be used for effective acetylene separation (Fig. 10).[85] The large-amplitude continuous breathing behavior of the C_2H_2 adsorption experiment proves that the intra-cage pores and inter-cage pores of the organic cage are the reasons for its high adsorption capacity and selectivity. However, for C_2H_4, its breathing behavior only comes from the inter-cage pores, which has been proved by adsorption experiments and molecular dynamics simulations. In addition, at 253 and 273 K, NKPOC-1-α adsorbs a large amount of C_2H_2 through the opening of a gate, while the amount of C_2H_4 adsorbed is negligible. Breakthrough experiments reveal that this flexible and robust material can effectively separate C_2H_2 from the C_2H_2/C_2H_4 mixture. In addition, NKPOC-1-α is the first POC with this function, and is expected to be used for industrial gas separation.

The removal of C_2H_6 from its analogue C_2H_4 is also crucial in the petrochemical industry, and their similar physical and chemical properties make their separation extremely challenging. The emerging POC materials for C_2H_6/C_2H_4 separation are still in their infancy. An example of a POC adsorbent (CPOC-301) based on octahedral calix[4]resorcinarene is reported,[86]

which can be used as a robust adsorbent to directly separate high-purity C_2H_4 from the C_2H_6/C_2H_4 mixture. Molecular simulation studies have shown that the excellent C_2H_6 selectivity is due to the suitable cage cavity in CPOC-301, which forms more multiple C–H···π and hydrogen bonds with C_2H_6 than C_2H_4. This work provides another new way for the highly selective separation of industrially important hydrocarbons using POCs.

Another design strategy for light hydrocarbon separation materials is to introduce POCs into the polymers to form a composite membrane. Because POCs are soluble in organic solvents, they can be mixed with polymers at the molecular level, which is more advantageous than traditional solid fillers. Based on this, the CC3 particles or CC3 molecules were uniformly distributed in the polymer to form a hierarchical transport channel membrane.[87] The membrane displays very fast C_3H_6 permeability (390 Barrer) and a good C_3H_6/C_3H_8 separation factor (12.1) through the C_3H_6 and C_3H_8 mixture (1/1, v/v) penetration test. More importantly, it also shows a stable separation effect in long-term tests, and has practical application potential in light hydrocarbon separation. Similarly, ionic liquids (ILs) were introduced into CC3 to construct an IL@CC3/PIM-1 membrane with the help of polymers of intrinsic microporosity (PIM), achieving effective separation of CO_2 and CH_4.[88] Doping ILs in the membrane can regulate the cavity size of POCs, enhance the solubility of CO_2, improve the compatibility of POCs and PIM, and further improve the diffusion selectivity, permeability and stability of the membrane. Compared with the CC3/PIM-1-10% membrane, the CO_2 permeability coefficient and CO_2/CH_4 selectivity of the membrane with ILs were increased by 15.9% and 106.2%, respectively. This provides a new idea for the separation of light hydrocarbons by POC-based membranes. In 2023, a composite membrane formed by POC (RCC3) cross-linked with terephthaloyl chloride (TPC) was proposed and constructed for the first time.[89] The pore size of RCC3 is about 5.4 Å with a high specific surface area of 442.3 $m^2 g^{-1}$, and imine-rich nanochannels are responsible for the rapid penetration of CO_2. In addition, the interfacial cross-linking reaction between RCC3 and TPC enables the TPC-RCC3 ultrathin film to be assembled on the surface of the modified polysulfone substrate. In addition, trace piperazine was further used to regulate the cross-linking degree of the ultra-thin film for improving the CO_2/N_2 selectivity. The prepared composite membrane has a high CO_2 permeance of 4303 GPU with a CO_2/N_2 selectivity of 30, and CH_4 permeance of 1216 GPU with a CH_4/N_2 selectivity of 3.0 at 1 bar, and can maintain permeation selectivity under long-term operation. Its excellent separation performance provides a more economical solution for CO_2 capture in flue gas or natural gas purification.

The cage-to-COF strategy can also be used to design new materials for the separation of light hydrocarbons. The Yuan group introduced different substituents on the linker to fine-tune the network conformation of the material to obtain three isostructural POC-based COF materials (3D-OC-COF-H, 3D-OC-COF-OH, and 3D-OC-COF-Cl),[90] as shown in Fig. 11. All three COFs exhibit high specific surface area compared to the precursor cage. Due to the unique pore environment and
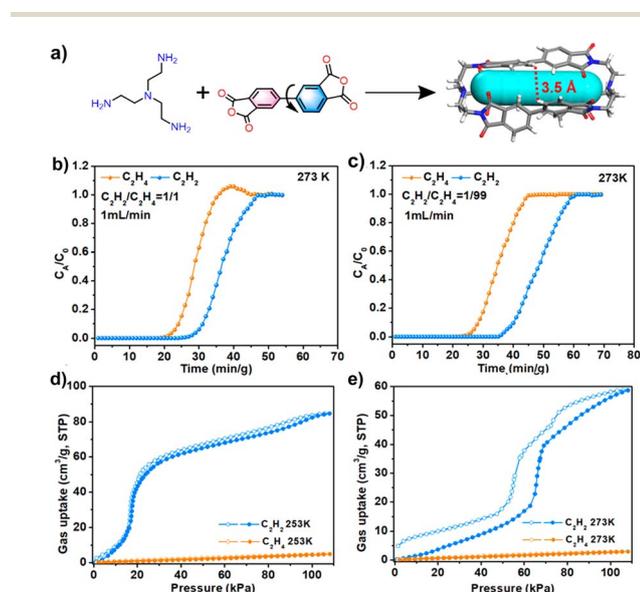

Fig. 10 (a) Synthesis of NKPOC-1; (b and c) adsorption–desorption isotherms of NKPOC-1-α for C_2H_2 and C_2H_4 at 253 and 273 K; (d and e) breakthrough curves of NKPOC-1-α for the C_2H_2/C_2H_4 mixture (1/99, v/v) and (50/50, v/v) with a gas flow of 1 mL min^{-1} at 273 K. Reproduced from ref. 85. Copyright 2023, The American Chemical Society.
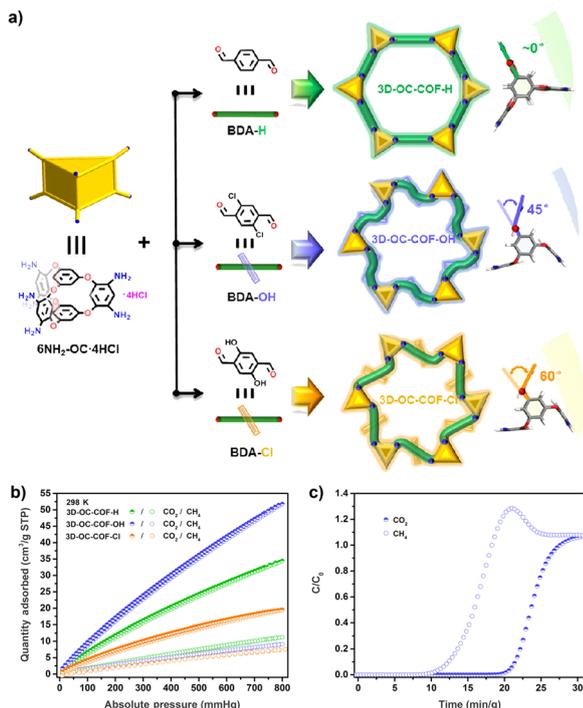
Fig. 11 (a) POC-based COFs containing different substituents; (b) N_2, CO_2, and CH_4 adsorptions of the three COFs at 298 K; (c) experimental column breakthrough curves for CO_2/CH_4 (50 : 50, v/v) of 3D-OC-COF-OH at room temperature. Reproduced from ref. 90. Copyright 2021, The Chinese Chemical Society.

different functional groups, 3D-OC-COF-OH exhibits excellent CO_2/CH_4 separation performance.

Rare gases are often used as protective gas or chemical raw materials in industrial production. The separation and purification of rare gases is a complex and high energy consumption process. POCs also have unique advantages in the separation of rare gases. In 2014, the separation of rare gases was realized using CC3.[91] The diameter of the internal cavity of the CC3 molecule is 4.4 Å, which is very similar to the diameter of the xenon (Xe) gas (4.1 Å). The narrowest diameter of the 3D channel formed by the stacking of adjacent cage molecules is 3.6 Å, slightly smaller than the diameter of krypton (Kr) (3.69 Å), which seems to hinder the diffusion of Xe or radon (Rn) gas. However, molecular dynamics simulations show that the flexible structure of CC3 molecules can lead to dynamic fluctuations in the pore size, which makes it possible to adsorb large-sized rare gases (including Kr, Xe and Rn) in a limited time range. Breakthrough experiments also confirm that CC3 can separate Kr, Xe and Rn from air at very low concentrations.

In 2020, the Carreon group successfully grew continuous CC3 composite membranes on alumina porous tubes and evaluated the performance of the membrane in the separation of Xe from light gases (He, CO_2, Kr and CH_4).[92] As a part of the membrane, CC3 is suitable for screening He, CO_2, Kr and CH_4 (kinetic pore size 2.6–3.8 Å). The dynamic diameter of Xe is 4.1 Å, which is larger than the maximum pore size of CC3, so the membrane can effectively separate Xe from light gas. In addition, the CC3 membrane has high gas permeability for He, CO_2,

Kr and CH_4, reaching 2114, 1705, 773 and 1962 GPU, respectively.

In the present case, the separation of D_2 and H_2 is mainly achieved by electrolysis of heavy water or low temperature distillation at 24 K, and the separation process is cumbersome, costly and energy-consuming. It is difficult for organic framework materials to screen D_2 and H_2 by finely adjusting the pore size. Small changes in the molecular structure of discrete POCs will have a profound impact on its solid accumulation. From the realization of the regulation of pore structure, POCs are expected to become the sorbent candidates for D_2 and H_2.[93] The strategy of organic synthesis was employed to regulate the internal cavity of the cage molecule, with "tying" of the diamine group with formaldehyde, acetone or acetaldehyde to realize ultrafine control over the cage cavity size. Combining small pore and large pore cages into a porous solid makes the material have high D_2/H_2 selectivity (8.0) and high D_2 absorption capacity (4.7 mmol g^{-1}).

The Vogel group elucidated the mechanism of different functionalizations in POCs to control the separation of D_2 and H_2 from the perspective of theoretical simulation.[94] By using *ab initio* molecular dynamics simulations, the specific mechanism of the interaction between RCC3, CC3-S and 6ET-RCC3 and hydrogen isotopes was clarified. Through the evaluation of multiple CC3-type POCs, the effects of temperature and functionalization on the movement of hydrogen isotopes were confirmed. This is expected to help realize the directional design of new materials that can be used for hydrogen isotope separation.

3.3.2 Liquid separation. The current chemical liquid separation technology also has the disadvantages of a complicated process, high cost and high energy consumption. Due to the similar structure and similar physical properties of some chemical products, it is necessary to adopt high energy-consuming separation processes based on vacuum distillation and extractive distillation, which brings new challenges to the global energy demand. Obviously, it is particularly important to seek a new alternative energy-saving separation technology. It is worth noting that POC materials are also widely used in the separation of a variety of valuable chemical liquids based on the porous structure and tunable pores of POCs.

As early as 2013,[95] the Cooper group used CC3 to separate C8 (such as xylene isomers) and C9 hydrocarbons (such as mesitylene and ethyltoluene isomers). Molecular simulation shows that linear molecules (*p*-xylene and 4-ethyltoluene) preferentially bind to CC3 molecules rather than other C8 and C9 isomers. Gas chromatography (GC) analysis showed that mesitylene passed through the CC3 column quickly, while 4-ethyltoluene was selectively retained in the column. This study reveals the unique advantages of POC materials in performing specific separation tasks. In 2016,[96] this group ultilized CC3 coated in a standard capillary column as a chromatographic stationary phase for GC separation of a series of mixtures, including aromatic compounds, racemic mixtures and hexane isomers. For the separation of hexane isomers, the separation effect of the CC3-based column was better than that of other commercially available GC columns. In 2020,[97] an azobenzene-

based organic cage (AZO-Cage) was reported to selectively separate steam and liquid state xylene isomers, with the highest selectivity among organic adsorbents. Although the crystal structure did not show a porous structure, the selective adsorption of *p*-xylene was achieved through the C–H···π interaction between the azo bonds in the AZO-Cage and the methyl hydrogens of the xylene. The material can also be regenerated under vacuum and reused. The Khashab group designed a triamine crystal molecule for the separation of styrene and ethylbenzene, and the selectivity of styrene was as high as 99%.[98] It was confirmed by DFT calculation that the planar styrene can be easily embedded in the cavity of triamine compared to ethylbenzene, thus showing excellent separation for styrene. A thienothiophene cage (ThT-cages) with adaptive porosity has been reported for the separation of cyclohexane from benzene in 2021.[99] The purity of cyclohexane selectively captured by ThT-cages from an equimolar benzene/cyclohexane mixture was 94%. This high selectivity is due to the multiple interactions between cyclohexane and thienothiophene ligands. In 2022, this group synthesized a cylindrical triamine macrocycle (P-TA) with a deeper cavity,[100] which can selectively capture 1-hexene from *trans*-3-hexene (selectivity > 84%), as shown in Fig. 12. This selective adsorption is produced by the formation of a thermodynamically stable host–guest complex between 1-hexene and P-TA. After that, this group designed a highly flexible 4,4′-oxybisbenzaldehyde-based cage (Oba-cage), which can selectively adsorb *ortho*-isomers from monohalotoluene isomers (X-toluene, X = F, Cl, Br), and the adsorption rate of *ortho*-bromotoluene is as high as 93%.[101] In addition, the adsorption rate of Oba-cage for these *ortho*-isomers increases with the increase in halogen substituents.

In practical applications, more industrial product separation scenarios involve more complex mixtures of ternary systems. For example, alkanes of different components are separated from crude oil. Graded molecular sieving, that is, using the same membrane to separate molecules of different sizes from a multivariate mixture, greatly reduces cost and energy consumption compared to using different techniques to screen different molecules. The POCs are prepared as a thin film material to regulate the selectivity of the membrane to different molecules to achieve graded molecular sieving.

The Cooper group prepared composite membranes by growing crystalline CC3 on a polyacrylonitrile carrier.[102] The membrane has ultrafast solvent permeability and a high rejection rate for organic dyes with a molecular weight greater than 600 g mol^{-1}. The pore size of the composite membrane can be switched to larger pores in methanol, and the molecular weight cut-off reaches 1400 g mol^{-1}. By changing the content of methanol, the composite membrane can be switched between two phases with different selectivities, which makes it possible to use a single membrane to screen the three organic dyes from the mixture. In 2022, the Sun group chemically crosslinked a series of cage-like molecules into flexible nanofilms with a thickness of 8 nm.[103] The composite membrane exhibits nanofluidic channels with excellent water permeability, and is superior to commercial nanofiltration membranes by 1–2 orders of magnitude. In addition, the membrane shows a photoresponsive gating effect, which can realize the separation of different organic dyes. In 2023, the Celebi group reported a hierarchically networked POC (CC3) membrane with dynamic pore control.[104] The cage membrane can reversibly adjust the pore size and selectivity through different solvents and ratios (water, methanol and DMF). The membrane can be effectively used for the separation of complex organic mixtures. A series of crystalline self-supporting POC films were obtained by interfacial polymerization design.[105] During the condensation of aldehydes and amines, intramolecular hydrogen bonds ensure the formation of a defect-free POC film. Powdery products are more easily obtained in organic cages without intramolecular hydrogen bonds. In addition, the obtained membranes showed high rejection for organic dyes in water and organic solvents. The membrane also has accurate screening ability in organic solvents.

3.4 Batteries

3.4.1 Lithium–sulfur batteries. Most portable consumer electronic products use lithium-ion batteries. Compared with traditional lead-acid batteries, lithium-ion batteries provide better energy performance and a lighter weight. However, due to the limited specific capacity of lithium-ion batteries (LIBs), it is difficult to meet some applications that require higher power and energy, such as electric vehicles. High specific capacity (>300 W h kg^{-1}) requires low-cost rechargeable battery systems for energy storage. Among all alternatives, lithium-sulfur batteries (LSBs) seem to be the most promising one because of their low cost, high abundance, and high theoretical specific capacity (2566 W h kg^{-1}), which is much higher than that of traditional lithium-ion batteries. However, LSBs have serious disadvantages, including low conductivity, volume expansion and polysulfide dissolution. In particular, the dissolution and
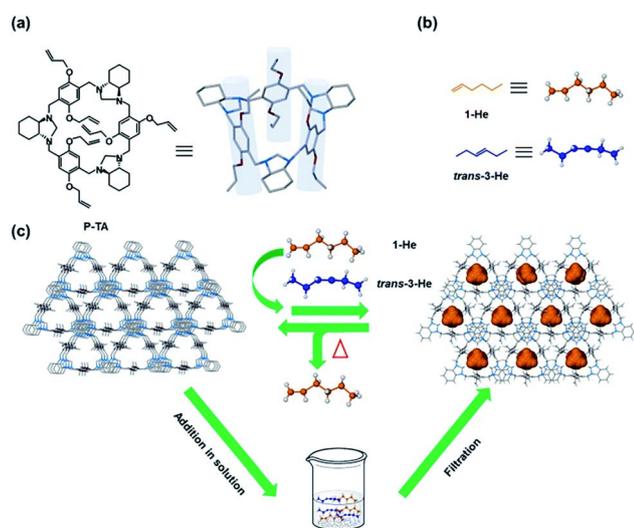
Fig. 12 (a) Chemical and crystal structures of P-TA; (b) linear hexene isomers; (c) schematic representation of selective hexene isomer separation by T-PA. Reproduced from ref. 100. Copyright 2023, The Royal Society of Chemistry.

shuttle of polysulfides lead to anode corrosion, low coulombic efficiency (CE) and rapid capacity decay, which limits the practical application of LSBs. POCs are used in cathodes and separators of LSBs due to their porous structure and fixation of sulfur or polysulfides. The POC-based cathodes of LSBs are mainly based on the porous structures and the active sites of sulfur adsorption inside the cages. In 2022, a naphthalene diimide-based porous POC (IIC-1) was developed to capture sulfides and used as a cathode for LSBs (Fig. 13a–e).[106] In aqueous solution, the electron-deficient skeleton of the cage exhibits good adsorption of electron-rich Na_2S_5 (490 mg g^{-1}) and the host–guest complex (IIC-1@Na_2S_5) exhibits typical sulfur charge–discharge plateaus of sulfur. As an anode, IIC-1@Na_2S_5 has a specific capacity of 852 mA h g^{-1} and good

stability, with only 0.05% per cycle after 1000 cycles. The immobilization of Na_2S_5 into IIC-1 makes the composite exhibit high cycle stability. POCs are also used as cathodes for LSBs. Based on the unique adsorption characteristics of cyclobenzoin ester as the host effective sulfur, a LSB with excellent electrochemical stability was designed by the Chung group.[108] The porosity and polar carbonyl group of cyclobenzoin ester provide an excellent chemical adsorption platform for polysulfides, and also realize the penetration of electrolyte. The LSB based on cyclobenzoin ester design has a low electrolyte sulfur ratio (4 µL mg^{-1}), high sulfur content (80 wt%), excellent discharge capacity (907 mA h g^{-1}) and high rate capability (C/20-1C). In this study, the porous molecular ring is used as a cathode to selectively adsorb polysulfides, which meets the two main
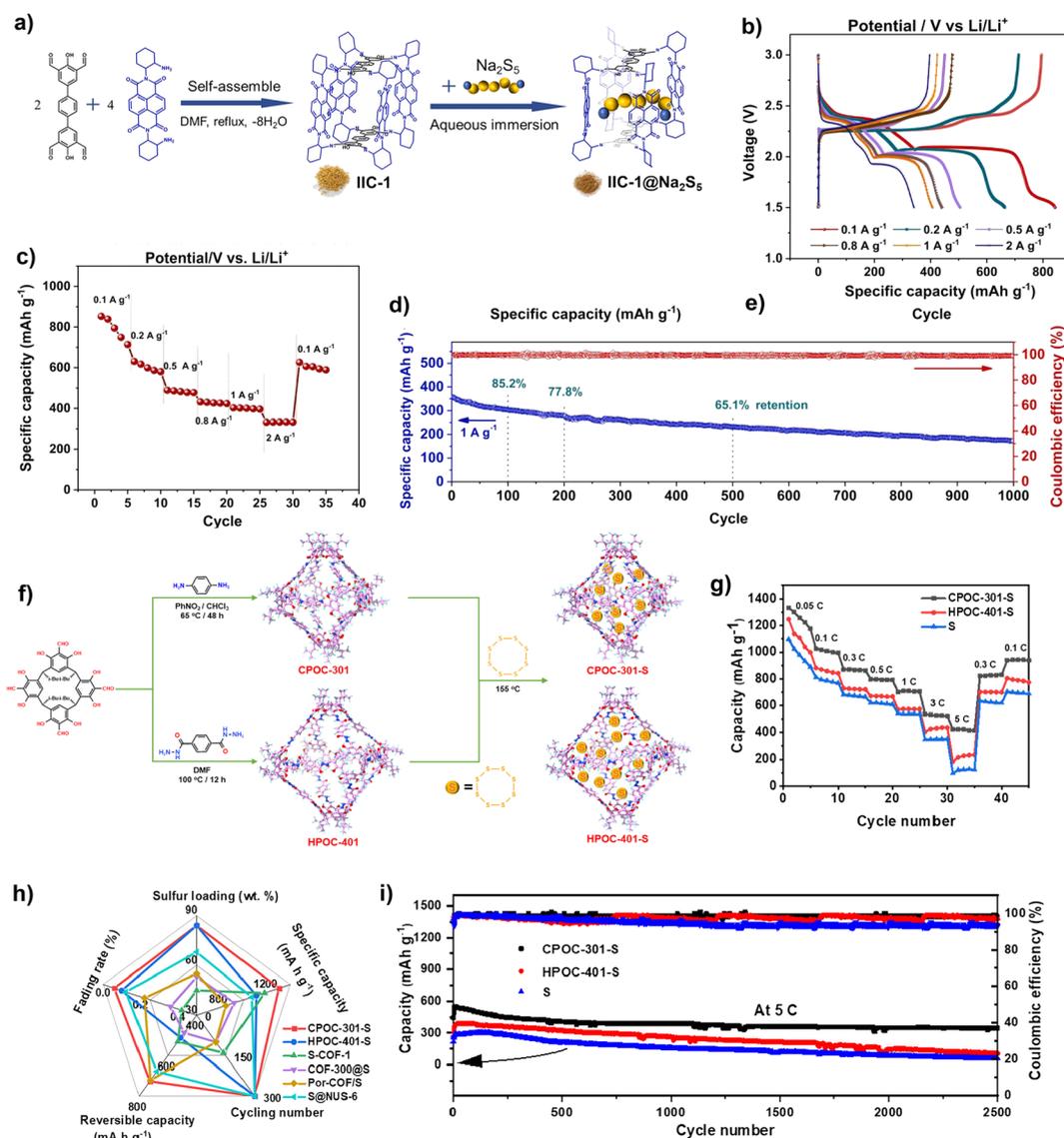
Fig. 13 (a) Synthesis of IIC-1 and the encapsulation of Na_2S_5; (b) galvanostatic charge/discharge profiles at different current densities; (c) rate performance; (d) cycling performance and CE. Reproduced from ref. 106. Copyright 2022, Elsevier. (e) Synthesis of CPOC-301, HPOC-401, CPOC-301-S and HPOC-401-S; (f) rate performance of S, CPOC-301-S, and HPOC-401-S; (g) cycling performance of S, CPOC-301-S, and HPOC-401-S; (h) comparison of the performance to that of other cathodes in LSBs; (i) cycling performance of S, CPOC-301-S and HPOC-401-S. Reproduced from ref. 107. Copyright 2023, The American Chemical Society.

requirements of a high-load sulfur cathode and thin electrolyte for high-energy-density LSBs. This study opens up a new strategy of selective chemical adsorption sulfur for lean-electrolyte LSBs that simultaneously optimize high active material loading and battery stability. In another example,[107] two POC materials, CPOC-301 and HPOC-401, with large cavities and abundant N and O heteroatoms, were used as host materials to accommodate a high sulfur content of 84 wt% in LSBs (Fig. 13f–i). The CPOC-301-S and HPOC-401-S based sulfur composite cathodes have improved electrochemical performance, high specific capacity (1302 and 1109 mA h g^{-1} at 0.05 C) and excellent cycle stability (the average capacity decay rate of CPOC-301-S at 5 C for 2500 cycles is 0.015%).

Compared with other reported MOFs and COFs, as shown in Table 2, the cathode based POC materials show comparable stability performance in LSBs. Although the specific capacity of IIC-1 and CE is relatively low, their cycle stabilities are not reduced due to the nature of the molecular material with a high percentage of the inert component. Even some POC materials have a cycle stability of more than MOFs and COFs, such as CPOC-301 can still maintain 63% of its initial capacity after 2500 cycles, and the specific capacity also reached 1302 mA h g^{-1}. Unfortunately, so far, there are only a few cases of the application of POCs in LSBs. The POC-based LSB materials, including the electrode, electrolyte and separation membrane, need to be further developed toward enhancing the corresponding performance.

Thin films with effective ion screening ability are in great demand in energy storage batteries. Another application of POCs is as a separator for LSBs. Solution processing into various devices is one of the advantages of POC materials. With this in mind, the Xie group reported a functional separator based on a POC (CC3) for fast and selective ion transport (Fig. 14).[117] The ion separation effect can be adjusted by using the design and preparation of the controllable thickness and porosity of the film. In this case, the functional separator assembled by using CC3 can selectively screen Li ions and effectively inhibit the production of unexpected polysulfides. The separator modified by using a POC film can lead to a battery with good cycling performance and rate performance. This new composite
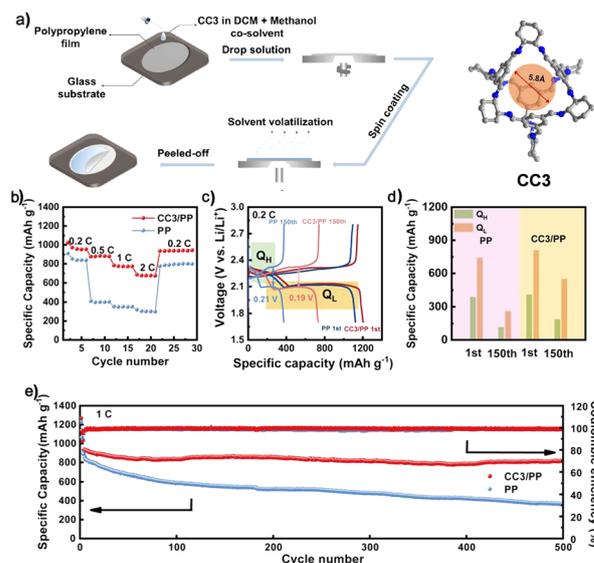

Fig. 14 (a) The fabrication process to produce CC3/PP separators; (b and c) rate performance and charge/discharge profiles of the batteries with different separators; (d) specific capacities of high-voltage plateaus (Q_H) and low-voltage plateaus (Q_L) for batteries with different separators; (e) cycling performance of batteries with different separators. Reproduced from ref. 117. Copyright 2022, The American Chemical Society.

separator made of soluble POCs and the PP shows broad prospects in high-performance energy storage devices.

3.4.2 Other lithium batteries. In addition to LSBs, LIBs have become one of the most important advances in energy storage technology in recent years due to their high energy density and operating voltage. The transport of lithium in the electrode is crucial to the performance of LIBs. The solid–liquid electrolyte nanocomposite system (SLEN) was prepared by the Gewirth group using POCs (Td_a) and LiTFSI-DME electrolyte solution.[118] The SLEN has excellent room temperature conductivity (1×10^{-3} S cm^{-1}) and low activation energy (16 kJ mol^{-1}). Cyclic voltammetry showed that the SLEN could maintain excellent oxidation stability at a voltage of up to 4.7 V, and also have good anode cycle stability. Coupled with the new application of POCs as functional materials, this material has great prospects in future electrochemical energy storage research. A new [3 + 6] triangular prism cage was obtained by condensation between tetraaldehyde (dibenzotetraazahexacene) and cyclohexanediamine.[119] The redox-active cage is used as the cathode material of LIBs, and its electrochemical performance (electrolytic stability, Li⁺ diffusion rate and capacity) is better than that of the monomer compound, which may be due to the lower solubility of the cage electrode in the electrolyte and the enhanced diffusion of lithium ions in the cage electrode.

Compared with liquid LIBs, all solid-state lithium batteries (SSLBs) have higher energy density and better safety, but the entire battery needs to have an effective ion conduction path. A POC-based ionic conductor, Li-RCC1-ClO_4, has been developed as a solid cathode for SSLBs (Fig. 15).[120] Due to the solution processability of POCs, Li-RCC1-ClO_4 can be dissolved in the

Table 2 Comparison of cathode performance of LSBs with POCs, COFs and MOFs

| Materials	Category	Specific capacity	Capacity retention	Ref.
IIC-1	POC	852 mA h g^{-1}	50% (1000 cycles)	106
CPOC-301	POC	1302 mA h g^{-1}	63% (2500 cycles)	108
CE	POC	907 mA h g^{-1}	52% (200 cycles)	107
HZ-DMTD	COF	642 mA h g^{-1}	79% (200 cycles)	109
3D-flu-COF	COF	1249 mA h g^{-1}	75% (1000 cycles)	110
TFPB-TAA	COF	1288 mA h g^{-1}	69% (400 cycles)	111
PI-COF	COF	1330 mA h g^{-1}	96% (100 cycles)	112
$Ni_3(HITP)_2$	MOF	1303 mA h g^{-1}	65% (100 cycles)	113
Cu-TDPAT	MOF	1675 mA h g^{-1}	56% (500 cycles)	114
Mn-CCs	MOF	1460 mA h g^{-1}	68% (200 cycles)	115
ZIF-8	MOF	1055 mA h g^{-1}	76% (300 cycles)	116
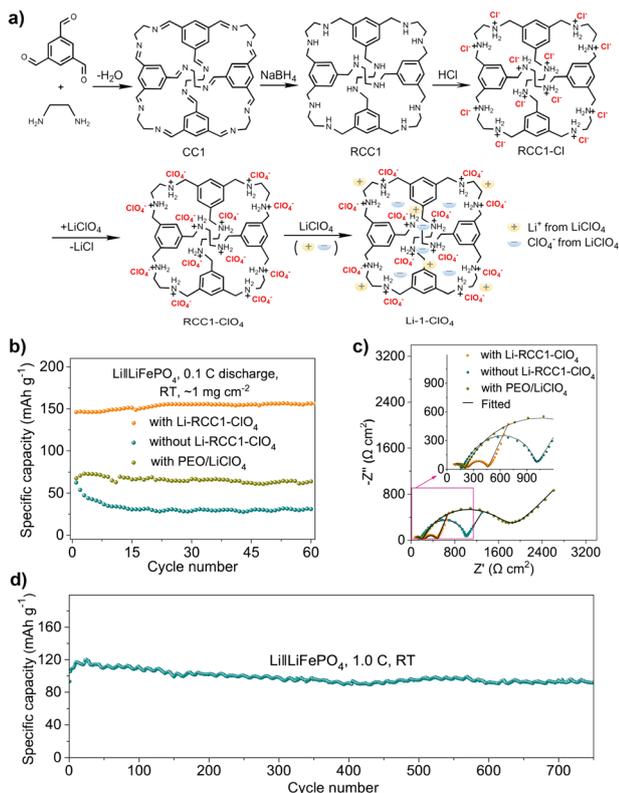
Fig. 15 (a) Synthetic procedure for the porous cage electrolyte, Li-RCC1-ClO$_4$; (b) cycling performance and (c) electrochemical impedance spectra profiles of the SSLBs at room temperature using LiFePO4 solid-state cathodes with different catholytes; (d) cycle performance of the all-solid-state cell with Li-RCC1-ClO$_4$. Reproduced from ref. 120. Copyright 2022, Springer Nature.

cathode slurry, which allows the use of traditional slurry coating methods to manufacture solid cathodes. This is often not possible for other insoluble porous solids, such as MOFs and COFs. The functional groups in the cavity of POC were ionized to provide an environment for efficient dielectric screening. Lithium ions and added lithium salts (such as LiClO$_4$) dissociated into mobile ions. These cage materials can uniformly dissolve in the cathode slurry, and grow and crystallize on the cathode surface during the coating process, and thereby an effective ion conduction network was formed inside the cathode. This employment of organic cages in SSLBs (the SSLBs containing 20% of Li-RCC1-ClO$_4$) can minimize ionic additives for the cathode, producing excellent cycling performance (capacity retention rate of 88.2% after 750 cycles) at room temperature.

Rechargeable Li–Cl$_2$ batteries are high energy density and safe energy storage batteries. Although the theoretical specific capacity is very high, the cycle life of the Li–Cl$_2$ battery is short and the CE is low due to the slow and insufficient supply of Cl$_2$ during the redox reaction. In order to solve this problem, an imine-functionalized POC was utilized as the cathode material of the Li–Cl$_2$ battery to capture Cl$_2$ molecules for achieving high discharge capacity and CE.[121] Density functional theory calculations show that the imine group sites in the host cage have

a strong interaction with Cl$_2$, which is conducive to the rapid capture of Cl$_2$. As a result, the capacity of the Li–Cl$_2$ battery using the POC (Li–Cl$_2$@POC) is significantly improved, and an ultra-high discharge capacity of 4000 mA h g^{-1} is achieved with 100% CE. The Li–Cl$_2$@POC battery exhibits excellent electrochemical performance even at low temperature. It can be stably cycled for 200 cycles at a capacity of 2000 m Ah g^{-1} at −20 °C, and the average CE is 99.7%.

Light-assisted LIBs are considered to be a promising technology that can simultaneously convert and store sunlight into electrochemical energy. However, there are still limitations in the design and synthesis strategies of photo-assisted organic cathodes for lithium-organic batteries. The Wang group reported a material composed of C$_{60}$ and POCs, C$_{60}$@POC, which can be used as a positive electrode for photo-assisted lithium-organic batteries to achieve efficient solar energy capture, conversion and storage (Fig. 16).[122] The structural characterization shows that the thermodynamic C$_{60}$ and POC are conducive to the formation of a complex with a host–guest stoichiometric ratio of 1 : 2. Optical and electrochemical analyses showed that C$_{60}$@POC not only enhanced charge generation/separation, but also accelerated the kinetics of the electrochemical lithium storage/release reaction compared with pristine POC. Under illumination, the battery based on the C$_{60}$@POC cathode shows excellent improved performance
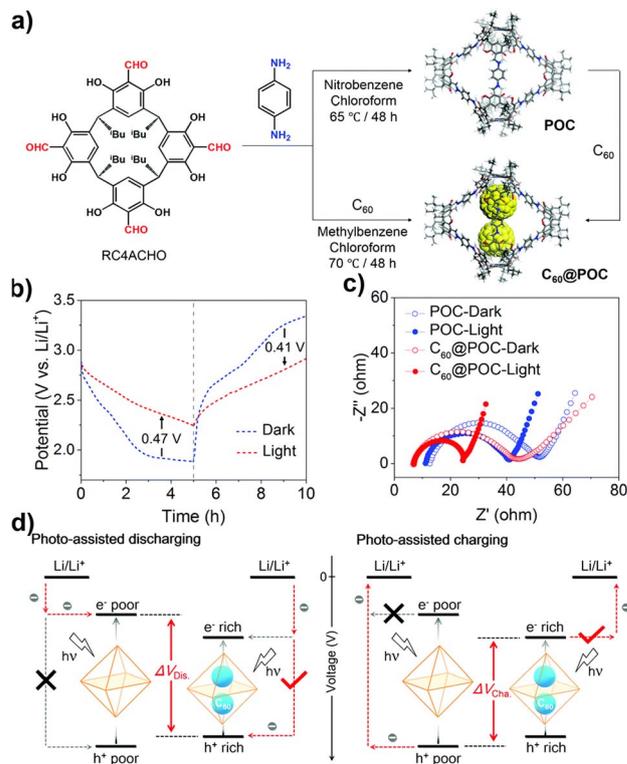

Fig. 16 (a) Schematic representation of the synthesis of POC and C60@POC; (b) charge and discharge curves of C60@POC with or without illumination; (c) Nyquist plots of POC and C60@POC with or without illumination; (d) schematic diagram of the photo-assisted Li-organic battery with POC and C60@POC cathodes. Reproduced from ref. 122. Copyright 2022, The Royal Society of Chemistry.
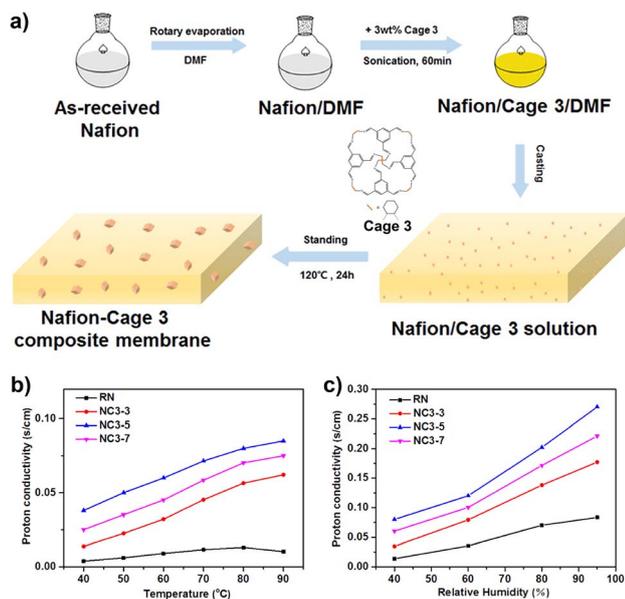
Fig. 17 (a) Schematic illustration of preparation of the Nafion−Cage 3 composite membrane; (b) temperature-dependent (40% RH) and (c) humidity-dependent (90 °C) proton conductivity of recast Nafion and the Nafion−Cage 3 composite membrane. Reproduced from ref. 125. Copyright 2018, The American Chemical Society.

including increasing output power, reducing input power, enhancing light conversion efficiency, and promoting efficient solar energy conversion and storage during charging and discharging. This example integrates the capture and conversion of light energy with the storage of chemical energy in POCs, which is helpful in expanding the application of more POCs in energy conversion and storage.

3.4.3 Perovskite solar batteries. Compared with energy storage lithium batteries, solar batteries can convert light energy into electrical energy. For perovskite solar cells (PSCs), buried interfaces with high concentrations of defects are crucial for efficient charge extraction to achieve high-performance devices. The Zhao group introduced a POC layer between SnO_2 and perovskite to spontaneously reconstruct the buried interface.[123] Through the multidentate chelation of POC and the chemical bonds formed by SnO_2 and perovskite, the buried interface greatly reduces the defect density and enhances the carrier extraction. More importantly, the study discloses that the iodide ions in the aging device migrate downward to the electron transport layer and even invade the ITO electrode, changing the corresponding work function. The host–guest interaction of POCs and iodide ions can effectively inhibit the downward migration of iodide ions. Therefore, the power conversion efficiency of PSCs fabricated by the POC recombination strategy is 24.13%. In addition, the restructured device with unencapsulated POC exhibits significantly improved long-term stability, maintaining 93% of its initial efficiency after 5000 hours.

3.5 Proton conductivity

Solid electrolytes for ion conduction have attracted extensive interest of researchers due to their wide application in energy
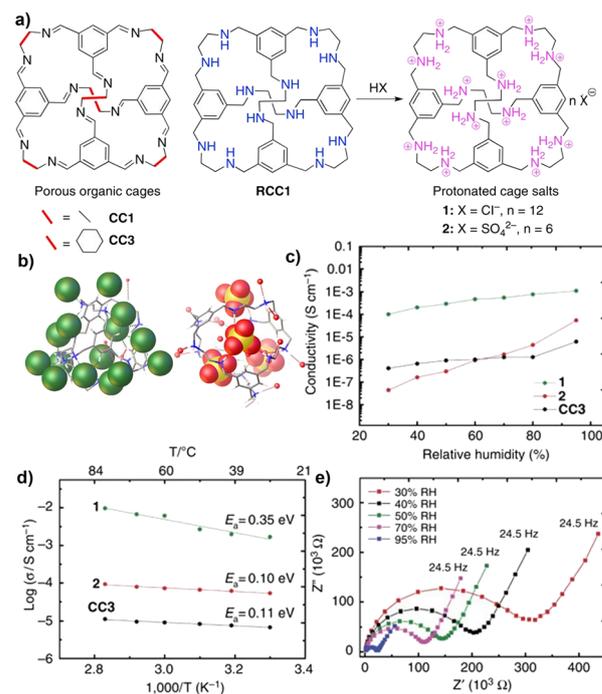

Fig. 18 (a) Molecular proton conductors based on neutral organic cage molecules and protonated cage salts; (b) the single-crystal structures of cage salts 1 and 2; (c) proton conductivities for salts 1 and 2, and neutral CC3 at 303 K as a function of relative humidity; (d) Arrhenius plots showing the activation energies of the cage materials; (e) Nyquist plots showing the impedance of CC3 at 303 K. Reproduced from ref. 126. Copyright 2016, Springer Nature.

fields such as fuel cells, flow batteries and LIBs. In recent years, crystalline porous framework materials such as MOFs and COFs have been widely studied due to their high porosity, high specific surface area and chemical functional groups. Unlike amorphous polymers, crystalline materials have tunable pore networks and regular frameworks, which make them potential candidates for proton conductivity. However, due to their poor machinability, it is still challenging to fabricate crystalline porous materials into mechanically stable films, which limits their proton conductivity properties. POCs are an emerging kind of porous molecular material. Due to the inherent channel structures and good machinability, POCs show great potential for proton conductivity.

A bottom-up strategy was proposed to obtain two different supramolecular conductors by self-assembly of Cage-1 (larger cavity size and more hydrogen bond anchors) and Cage-2 (small cavity size and fewer hydrogen bond anchors) with the same chemical composition but different structural characteristics.[124] Cage-1 is self-assembled to form a crystalline phase with a proton hopping path. The proton conductivity is based on the Grotthuss mechanism, and the proton conductivity is 1.59×10^{-4} S cm^{-1}. The proton conductivity of Cage-2 is based on the vehicle mechanism. Its proton conductivity is about 1/200 of the former. Theoretical simulation reveals the different hydrogen bond dynamics in Cage-1 and Cage-2, which provides further insights into the potential proton diffusion mechanism.

A soluble POC (cage 3) was fabricated into a proton exchange membrane by *in situ* crystallization, obtaining a composite proton exchange membrane.[125] The crystalline cage 3 dispersed in the Nafion matrix has an inherent three-dimensional inter-connected proton pathway, which promotes the proton conductivity of the proton-exchange membrane (Fig. 17). Due to the multiple hydrogen bond interactions between cage 3 and Nafion, more continuous proton pathways are constructed. In addition, cage 3 has high water absorption, and the retention of membrane moisture ensures proton transfer at low humidity. The prepared membranes show higher proton conductivity than cast Nafion under both low and high humidity conditions. The proton conductivity of the Nafion–Cage 3 membrane reaches 0.27 S cm^{-1} at 90 °C and 95% relative humidity, which is much higher than that of the recast Nafion (0.08 S cm^{-1}) under the same conditions.

A POC-based salt was developed to construct proton-transporting crystalline porous molecular solids with 3D channel structures (Fig. 18).[126] For the neutral imine cage CC3, there is a hydrated 3D pore network in the material, but the proton conductivity is relatively low under wet conditions. RCC1 is obtained by reducing CC3 and then transforming it into a crystalline hydrated salt, $(H_{12}RCC1)^{12+} \cdot 12Cl^{-} \cdot 4H_2O$, the proton conductivity is significantly increased by more than 150 times, and its proton conductivity is even comparable to that of proton-conducting MOFs. For $(H12RCC1)^{12+} \cdot 6(SO_4)^{2--} \cdot 27.25(H_2O)$, the larger radius of $(SO_4)^{2-}$ introduced limits the diffusion of water, making the effect of RH on its proton conductivity more significant.

4 Conclusions and outlook

The continuous development of advanced materials with new structures and functions is crucial for energy applications. In this perspective, we comprehensively review the latest advances in the applications of pristine POCs, POC composites and POC derivatives in energy applications, including photo-catalysis, electrocatalysis (NO$_3$RR, OER, HER, ORR and CO$_2$RR), separation (gas separation and liquid separation), batteries (LSBs, other lithium batteries and perovskite solar batteries) and proton conductivity, as shown in Table 3. (1) Pristine POCs with microporous structures and abundant active sites have been used in separation, solar energy capture, batteries, *etc.*, and achieved good performance. (2) POC composites integrated with POCs and functional components have been explored and efficiently utilized in photocatalysis, electrocatalysis, and batteries. POC composites can not only make up for the shortcomings of poor conductivity of original POCs, but also realize the synergistic effect between POCs and functional units, resulting in customized performance. (3) POC derivative materials, including COFs, MOFs, HOFs and other materials, have more abundant pores, higher stability and more exposed functional active sites, showing enhanced performance in many fields such as adsorption separation and catalysis. In summary, more energy-related applications can be achieved by using POCs, further strengthening and expanding their functionality.

Although great progress has been made in energy applications, POC-based materials are in their infancy and more efforts should be invested in the following areas. (1) The stability of pristine POCs is the main problem in the application of photoelectric and electrochemical energy due to the metastable imine bonds for most cages, and its performance needs to be further improved towards the practical application. For example, some reasonable design strategies can be used to develop more stable POCs, such as converting revers-ible bonds into irreversible bonds through post-modification, and adjusting the hydrophilicity and hydrophobicity of mate-rials. In addition, the structure of the original POCs can also be optimized, such as the introduction of new groups, hetero-atom doping, and pore size regulation. (2) The development of simpler and greener POC synthesis methods for scalable production, such as mechanical grinding synthesis and aqueous synthesis strategies, to achieve universal synthesis of POC-based materials, thereby reducing costs and reducing environmental pollution. (3) POC-based composites should be further developed, not only limited to the combination with MNPs, but also to explore more functional components, such as organic small molecules, enzymes, and even inorganic semiconductors. Through new synthesis methods, the func-tional diversity of POC composites materials is enriched. (4) Compared with powder materials, the corresponding devices are closer to practical applications. For example, POCs are converted into a film to achieve efficient gas separation or proton conductivity, so more efforts should be devoted to device manufacturing. (5) How to further improve the perfor-mance of POCs in energy applications? For electrocatalysis, although the catalytic performance of POCs has reached a high level in the lab, it still needs to be further improved for reaching the standard of commercial products. In addition, increasing the specific surface area and porosity of POCs may also improve the pore-related performance of POCs in the energy field. From the perspective of POCs' structure design and transformation into POC derivatives, the synthesis of nanoscale POC solid materials may be beneficial to improve their performance. (6) Advanced characterization techniques (*e.g.*, crystal structure characterization is an important basis for the structure of POCs, and *in situ* characterization is crucial for mechanism research) and theoretical calculations are essential as powerful tools to systematically study the trans-formation process and related mechanisms in POC-based materials, including micro-component changes, kinetic and thermodynamic processes, and possible synergy between multiple components.

Indeed, opportunities and challenges coexist in developing POCs for energy applications, and pioneering studies are very urgently desired. In the present case, most of the research studies are still in the laboratory stage, and large-scale practical promotion is encouraged. There is still a long way for practical applications of POC-based materials in energy applications. POC-based materials have made great progress in structural design and application, which is indeed exciting. Therefore, we believe that the application of POC-based materials in the energy field will have bright prospects through the mutual

Table 3 Overview of the energy applications and performances of some typical POC based materials

POC	Category	Applications	Performance	Ref.
Zn-PB	Pristine POCs	Photocatalysts	Photooxidation of 1,5-dihydroxynaphthalene	57
P$_{12}$L$_{24}$	Pristine POCs	Photocatalysts	Photooxidation of 1,5-dihydroxynaphthalene	58
PTC-1(2H)	Pristine POCs	Photocatalysts	Photooxidation of amines to imines (99% conversion, TOF > 33 h^{-1})	59
PyTC1	Pristine POCs	Photocatalysts	Photooxidation of benzeneboronic acid to phenols (99% conversion)	60
Pd@MTC1-1/5	POC composites	Photocatalysts	Photooxidation of 4-nitrophenylboronic acid to 4-aminophenol	51
Green box 5	Pristine POCs	Photocatalysts	Photocatalytic hydrogen production (34 μmol h^{-1})	62
FePB-3(N)	Pristine POCs	Photocatalysts	Photocatalytic reduction of CO$_2$ (97% selectivity; TON > 1100 h^{-1})	63
TPPCage-8I	Pristine POCs	Photocatalysts	Photooxidation of amines to imines (99% conversion; TOF > 1980 h^{-1})	65
CoP@POC	Pristine POCs	Photocatalysts	Photooxidation of amines to imines (99% conversion; TOF > 1389 h^{-1})	64
Au@OC1^R	POC composites	Photocatalysts	Nitrobenzene to the azo compound (92% yield; TOF > 9200 h^{-1})	66
Ag@CC3-OH	POC composites	Photocatalysts	Nitrobenzene to the azo compound (99% conversion; TOF > 9200 h^{-1})	67
Au@TAE-DTE	POC composites	Photocatalysts	Photocatalytic reduction of CO$_2$ (56.4 μmol g^{-1} h^{-1} under visible light)	68
Ag^0@OB4^R	POC composites	Photocatalysts	Ullmann-type coupling reaction (63–95% yield)	69
Pd5-PS	POC composites	Photocatalysts	Photocatalytic reduction of CO$_2$ (98% CH$_4$ selectivity; 78.5 μmol g^{-1} h^{-1})	70
PSS-1	POC derivatives	Photocatalysts	Photooxidation of 1,5-dihydroxynaphthalene	57
Fe-PB	Pristine POCs	Electrocatalysis	Electrochemical CO$_2$ to CO (TOF of 0.64 s^{-1} at −0.63 V, 100% FE)	75
CPOC-Co	Pristine POCs	Electrocatalysis	Electrochemical CO$_2$ to CO (current density of 18.0 mA cm^{-2} at −0.90 V; 90% FE)	76
ZnPc	Pristine POCs	Electrocatalysis	Electrochemical CO$_2$ to CO (TOF of 606 h^{-1} at −1.3 V; >95% FE)	77
Cu-nr/CC3	POC composites	Electrocatalysis	Electrochemical CO$_2$ to C^{2+} (current density of 1.7 A cm^{-2} at −0.90 V; 76.1% FE)	78
CoPB-1(8)	Pristine POCs	Electrocatalysis	Electrochemical NO$_3^-$ to ammonia (TOF of 56 s^{-1} at −1.54 V; 90% FE)	79
Co-rPB-1(6)	Pristine POCs	Electrocatalysis	Electrochemical ORR ($E_{cat/2}$ of 0.48 V; 90% FE)	80
Co-PB-1	Pristine POCs	Electrocatalysis	Electrochemical HER (Tafel slope of 119 mV per decade; 100% FE; TOF of 0.22 s^{-1})	81
Cage-COF-1-Ns/Co	POC derivatives	Electrocatalysis	Electrochemical OER (Tafel slope of 56 mV per decade; overpotential of 330 mV)	82
CPOC-101α	Pristine POCs	C$_2$H$_2$/CO$_2$ separation	Selectivity of 11.9 and separation factor of 2.2	83
CPOC-107	Pristine POCs	C$_2$H$_2$/CO$_2$ separation	C$_2$H$_2$ adsorption value of 146 cm^3 g^{-1} at 298 K; breakthrough time of 13 min g^{-1}	84
NKPOC-1-α	Pristine POCs	C$_2$H$_2$/C$_2$H$_4$ separation	C$_2$H$_2$ adsorption value of 58 cm^3 g^{-1} at 273 K; breakthrough time of 16 min g^{-1}	85
CPOC-301	Pristine POCs	C$_2$H$_6$/C$_2$H$_4$ separation	C$_3$H$_6$ adsorption value of 87 cm^3 g^{-1} at 293 K; separation factor of 1.3	86
CC3@MMM	POC composites	C$_3$H$_6$/C$_3$H$_8$ separation	C$_3$H$_6$ permeability of 390 Barrer; separation factor of 12.1	87
IL@CC3/PIM-1-10%	POC composites	CO$_2$/CH$_4$ separation	CO$_2$ permeability of 7868 Barrer; CO$_2$/CH$_4$ selectivity of 73.4	88
TPC-RCC3	Pristine POCs	CO$_2$/N$_2$ separation	CO$_2$ permeance of 4303 GPU; CO$_2$/N$_2$ selectivity of 30	89
3D-OC-COF-OH	POC derivatives	CO$_2$/CH$_4$ separation	CO$_2$ capacity of 89.2 cm^3 g^{-1} at 273 K; CO$_2$ Q_{st} of 22.4 kJ mol^{-1}	90
CC3	POC composites	Xe/Kr/Rn separation	Xenon retained time > 15 min; flow rate of 40 cm^3 STP per min	91
CC3 membranes	Pristine POCs	He/CO$_2$/Kr/CH$_4$/Xe separation	He permeability of 2114 GPU; He/Xe ideal selectivity of 13	92
6FT-RCC3	Pristine POCs	D$_2$/H$_2$ separation	D$_2$/H$_2$ selectivity of 8.0; high D$_2$ absorption capacity of 4.7 mmol g^{-1}	94
CC3	Pristine POCs	C8/C9 separation	Mesitylene from C8/C9 isomers	95
CC3-R	Pristine POCs	Hexane separation	Reusability > 300 injections	96
AZO-cage	Pristine POCs	C8 separation	p-Xylene from C8 isomers	97
Macrocycle 1	Pristine POCs	Styrene/ethylbenzene separation	Styrene selectivity of 99%	98
ThT-cages	Pristine POCs	Benzene/cyclohexane separation	Cyclohexane selectivity of 94%	99
P-TA	Pristine POCs	1-Hexene/trans-3-hexene separation	1-Hexene selectivity of selectivity > 84%	100
Oba-cage	Pristine POCs	Monohalotoluene separation	Ortho-bromotoluene selectivity of 93%	101
CC3 composite membranes	POC composites	Organic dye separation	Molecular weight cut-off of 1400 g mol^{-1}	102
IIC-1	Pristine POCs	Cathode of LSBs	Discharge capacity of 852 mA h g^{-1}; capacity retention of 50% (1000 cycles)	106
CE	Pristine POCs	Cathode of LSBs	Discharge capacity of 970 mA h g^{-1}; capacity retention of 52% (100 cycles)	108
CPOC-301	Pristine POCs	Cathode of LSBs	Discharge capacity of 1302 mA h g^{-1}; capacity retention of 32% (2500 cycles)	107
CC3/PP	POC composites	Separator of LSBs	Discharge capacity of 956 mA h g^{-1}; capacity retention of 80% (500 cycles)	117

Table 3 (Contd.)

POC	Category	Applications	Performance	Ref.
SLEN	POC composites	Ionic conductivity	Ionic conductivity of 1×10^{-3} S cm^{-1}; low activation energy of 16 kJ mol^{-1}	118
Cage 1	Pristine POCs	Cathode of LIBs	Discharge capacity of 83 mA h g^{-1}; capacity retention of 34% (100 cycles)	119
Li-RCC1-ClO$_4$	Pristine POCs	Cathode of SSLBs	Discharge capacity of 122–135 mA h g^{-1}; capacity retention of 75% (882 cycles)	120
Li-Cl$_2$@POC	POC composites	Cathode of Li-Cl$_2$ batteries	Discharge capacity of 2000 mA h g^{-1} at −20 °C; CE of 99.7%	121
C$_{60}$@POC	POC composites	Cathodes of lithium-organic batteries	Charge separation efficiency ($t_{CS/CR}$ = 20.83/171.17); solar energy conversion efficiency of ~1%	122
POC@PbI$_2$	POC composites	Perowskite solar cells	Power conversion efficiency of 24.13%; efficiency retention of 93% (5000 cycles)	123
Cage-1-TREN	Pristine POCs	Proton conductivity	Proton conductivity of 1.59×10^{-4} S cm^{-1}	124
Nafion–Cage 3	POC composites	Proton conductivity	Proton conductivity of 0.27 S cm^{-1}	125
(H$_{12}$RCC1)$^{12+}$·12Cl$^-$·4H$_2$O	POC composites	Proton conductivity	Proton conductivities of 10^{-3} S cm^{-1}	126

promotion of structural design, structural regulation and theoretical calculation.

Data availability

No primary research results, software or code have been included and no new data were generated or analysed as part of this review.

Author contributions

All the authors wrote the perspective together.

Conflicts of interest

There are no conflicts to declare.

Acknowledgements

Notes and references

1 X. Yang, Z. Ullah, J. F. Stoddart and C. T. Yavuz, *Chem. Rev.*, 2023, **123**, 4602–4634.

2 G. Zhang and M. Mastalerz, *Chem. Soc. Rev.*, 2014, **43**, 1934–1947.

3 H. Wang, Y. Jin, N. Sun, W. Zhang and J. Jiang, *Chem. Soc. Rev.*, 2021, **50**, 8874–8886.

4 G. Montà-González, F. Sancenón, R. Martínez-Máñez and V. Martí-Centelles, *Chem. Rev.*, 2022, **122**, 13636–13708.

5 R. A. Borse, Y. Tan, D. Yuan and Y. Wang, *Energy Environ. Sci.*, 2024, **17**, 1307–1329.

6 M. Wilms, L. V. Melendez, R. J. Hudson, C. R. Hall, S. P. Ratnayake, T. Smith, E. D. Gaspera, G. Bryant, T. U. Connell and D. E. Gómez, *Angew. Chem., Int. Ed.*, 2023, **62**, e202303501.

7 P. Bhandari and P. S. Mukherjee, *ACS Catal.*, 2023, **13**, 6126–6143.

8 H. Guo, Y. Liu, H. Dong, W. Zong, K. Chu, W. Li, Z. Fan, G. He, Y. Miao, I. P. Parkin, F. Lai and T. Liu, *Sci. Bull.*, 2022, **67**, 2428–2437.

9 A. P. Côté, A. I. Benin, N. W. Ockwig, M. O'Keeffe, A. J. Matzger and O. M. Yaghi, *Science*, 2005, **310**, 1166–1170.

10 W. Zhao, Q. Zhu, X. Wu and D. Zhao, *Chem. Soc. Rev.*, 2024, **53**, 7531–7565.

11 R. Liu, K. T. Tan, Y. Gong, Y. Chen, Z. Li, S. Xie, T. He, Z. Lu, H. Yang and D. Jiang, *Chem. Soc. Rev.*, 2021, **50**, 120–242.

12 H. Lin, Y. Yang, Y. Hsu, J. Zhang, C. Welton, I. Afolabi, M. Loo and H. Zhou, *Adv. Mater.*, 2024, **36**, 2209073.

13 H. Jin, P. Zhao, Y. Qian, J. Xiao, Z. Chao and H. Jiang, *Chem. Soc. Rev.*, 2024, **53**, 9378–9418.

14 R. Lin, Y. He, P. Li, H. Wang, W. Zhou and B. Chen, *Chem. Soc. Rev.*, 2019, **48**, 1362–1389.

15 L. Shi, Z. Xiong, H. Wang, H. Cao and Z. Chen, *Chem*, 2024, **10**, 2464–2472.

16 Q. Zhu, L. Wei, C. Zhao, H. Qu, B. Liu, T. Fellowes, S. Yang, A. Longcake, M. J. Hall, M. R. Probert, Y. Zhao, A. I. Cooper and M. A. Little, *J. Am. Chem. Soc.*, 2023, **145**, 23352–23360.

17 K. Cheng, H. Li, Z. Li, P. Li and Y. Zhao, *ACS Mater. Lett.*, 2023, **5**, 1546–1555.

18 Q. Zhu, X. Wang, R. Clowes, P. Cui, L. Chen, M. A. Little and A. I. Cooper, *J. Am. Chem. Soc.*, 2020, **142**, 16842–16848.

19 J. Ma, J. Li, Y. Chen, R. Ning, Y. Ao, J. Liu, J. Sun, D. Wang and Q. Wang, *J. Am. Chem. Soc.*, 2019, **141**, 3843–3848.

20 X. Ding, B. Han, B. Yu, H. Wang and J. Jiang, *Sci. China: Chem.*, 2023, **66**, 2019–2027.

21 Y. Jin, Q. Wang, P. Taynton and W. Zhang, *Acc. Chem. Res.*, 2014, **47**, 1575–1586.

22 T. Tozawa, J. T. A. Jones, S. I. Swamy, S. Jiang, D. J. Adams, S. Shakespeare, R. Clowes, D. Bradshaw, T. Hasell, S. Y. Chong, C. Tang, S. Thompson, J. Parker, A. Trewin, J. Bacsa, A. M. Z. Slawin, A. Steiner and A. I. Cooper, *Nat. Mater.*, 2009, **8**, 973–978.

23 K. Acharyya and P. S. Mukherjee, *Angew. Chem., Int. Ed.*, 2019, **58**, 8640–8653.

24 X. Dong, H. Qu, A. C. H. Sue, X. Wang and X. Cao, *Acc. Chem. Res.*, 2024, **57**, 1111–1122.

25 J. Kou, W. D. Wang, J. Fang, F. Li, H. Zhao, J. Li, H. Zhu, B. Li and Z. Dong, *Appl. Catal., B*, 2022, **315**, 121487.

26 C. Liu, W. Li, Y. Liu, H. Wang, B. Yu, Z. Bao and J. Jiang, *Chem. Eng. J.*, 2022, **428**, 131129.

27 H. Ren, C. Liu, X. Ding, X. Fu, H. Wang and J. Jiang, *Chin. J. Chem.*, 2022, **40**, 385–391.

28 W. Liu and J. F. Stoddart, *Chem*, 2021, **7**, 919–947.

29 K. G. Andrews, T. K. Piskorz, P. N. Horton and S. J. Coles, *J. Am. Chem. Soc.*, 2024, **146**, 17887–17897.

30 M. Zhang, Z. He, L. Wang, X. Zhang and G. Li, *Small*, 2024, **20**, 2308400.

31 S. Zhang, Z. Kochovski, H. Lee, Y. Lu, H. Zhang, J. Zhang, J. Sun and J. Yuan, *Chem. Sci.*, 2019, **10**, 1450–1456.

32 C. Liu, Y. Jin, D. Qi, X. Ding, H. Ren, H. Wang and J. Jiang, *Chem. Sci.*, 2022, **13**, 7014–7020.

33 H. Li, H. Zhang, A. D. Lammer, M. Wang, X. Li, V. M. Lynch and J. L. Sessler, *Nat. Chem.*, 2015, **7**, 1003–1008.

34 Y. Horng, T. Lin, C. Tu, T. Sung, C. Hsieh, C. Hu, H. M. Lee and T. Kuo, *Eur. J. Org Chem.*, 2009, **2009**, 1511–1514.

35 C. Zhang, Q. Wang, H. Long and W. Zhang, *J. Am. Chem. Soc.*, 2011, **133**, 20995–21001.

36 Q. Wang, C. Zhang, B. C. Noll, H. Long, Y. Jin and W. Zhang, *Angew. Chem., Int. Ed.*, 2014, **53**, 10663–10667.

37 J. Taesch, V. Heitz, F. Topić and K. Rissanen, *Chem. Commun.*, 2012, **48**, 5118–5120.

38 S. Ivanova, E. Köster, J. J. Holstein, N. Keller, G. H. Clever, T. Bein and F. Beuerle, *Angew. Chem., Int. Ed.*, 2021, **60**, 17455–17463.

39 F. Qiu, X. Chen, W. Wang, K. Su and D. Yuan, *CCS Chem.*, 2023, **6**, 149–156.

40 J. Zhang, Y. Li, W. Yang, S. Lai, C. Zhou, H. Liu, C. Che and Y. Li, *Chem. Commun.*, 2012, **48**, 3602–3604.

41 Z. Wang, H. Ma, T. Zhai, G. Cheng, Q. Xu, J. Liu, J. Yang, Q. Zhang, Q. Zhang, Y. Zheng, B. Tan and C. Zhang, *Adv. Sci.*, 2018, **5**, 1800141.

42 R. Kaur, S. Sen, M. C. Larsen, L. Tavares, J. Kjelstrup-Hansen, M. Ishida, A. Zieleniewska, V. M. Lynch, S. Bähring, D. M. Guldi, J. L. Sessler and A. Jana, *J. Am. Chem. Soc.*, 2020, **142**, 11497–11505.

43 W. Liu, C. Lin, J. A. Weber, C. L. Stern, R. M. Young, M. R. Wasielewski and J. F. Stoddart, *J. Am. Chem. Soc.*, 2020, **142**, 8938–8945.

44 A. Avellaneda, P. Valente, A. Burgun, J. D. Evans, A. W. Markwell-Heys, D. Rankine, D. J. Nielsen, M. R. Hill, C. J. Sumby and C. J. Doonan, *Angew. Chem., Int. Ed.*, 2013, **52**, 3746–3749.

45 A. S. Bhat, S. M. Elbert, W. Zhang, F. Rominger, M. Dieckmann, R. R. Schröder and M. Mastalerz, *Angew. Chem., Int. Ed.*, 2019, **58**, 8819–8823.

46 J. T. A. Jones, D. Holden, T. Mitra, T. Hasell, D. J. Adams, K. E. Jelfs, A. Trewin, D. J. Willock, G. M. Day, J. Bacsa, A. Steiner and A. I. Cooper, *Angew. Chem., Int. Ed.*, 2011, **50**, 749–753.

47 C. J. Pugh, V. Santolini, R. L. Greenaway, M. A. Little, M. E. Briggs, K. E. Jelfs and A. I. Cooper, *Cryst. Growth Des.*, 2018, **18**, 2759–2764.

48 T. Hasell, X. Wu, J. T. A. Jones, J. Bacsa, A. Steiner, T. Mitra, A. Trewin, D. J. Adams and A. I. Cooper, *Nat. Chem.*, 2010, **2**, 750–755.

49 S. Jiang, K. E. Jelfs, D. Holden, T. Hasell, S. Y. Chong, M. Haranczyk, A. Trewin and A. I. Cooper, *J. Am. Chem. Soc.*, 2013, **135**, 17818–17830.

50 S. Jiang, J. T. A. Jones, T. Hasell, C. E. Blythe, D. J. Adams, A. Trewin and A. I. Cooper, *Nat. Commun.*, 2011, **2**, 207.

51 N. Sun, C. Wang, H. Wang, L. Yang, P. Jin, W. Zhang and J. Jiang, *Angew. Chem., Int. Ed.*, 2019, **58**, 18011–18016.

52 B. Han, H. Wang, C. Wang, H. Wu, W. Zhou, B. Chen and J. Jiang, *J. Am. Chem. Soc.*, 2019, **141**, 8737–8740.

53 Q. Song, J. Yang, K. Zheng, T. Zhang, C. Yuan, L. Yuan and X. Hou, *J. Am. Chem. Soc.*, 2024, **146**, 7594–7604.

54 Z. Shan, X. Wu, B. Xu, Y. Hong, M. Wu, Y. Wang, Y. Nishiyama, J. Zhu, S. Horike, S. Kitagawa and G. Zhang, *J. Am. Chem. Soc.*, 2020, **142**, 21279–21284.

55 A. Giri, G. Shreeraj, T. K. Dutta and A. Patra, *Angew. Chem., Int. Ed.*, 2023, **62**, e202219083.

56 C. Liu, Y. Jin, Z. Yu, L. Gong, H. Wang, B. Yu, W. Zhang and J. Jiang, *J. Am. Chem. Soc.*, 2022, **144**, 12390–12399.

57 Y. Kim, J. Koo, I. Hwang, R. D. Mukhopadhyay, S. Hong, J. Yoo, A. A. Dar, I. Kim, D. Moon, T. J. Shin, Y. H. Ko and K. Kim, *J. Am. Chem. Soc.*, 2018, **140**, 14547–14551.

58 J. Koo, I. Kim, Y. Kim, D. Cho, I. Hwang, R. D. Mukhopadhyay, H. Song, Y. H. Ko, A. Dhamija,

H. Lee, W. Hwang, S. Kim, M. Baik and K. Kim, *Chem*, 2020, **6**, 3374–3384.

59 C. Liu, K. Liu, C. Wang, H. Liu, H. Wang, H. Su, X. Li, B. Chen and J. Jiang, *Nat. Commun.*, 2020, **11**, 1047.

60 N. Sun, D. Qi, Y. Jin, H. Wang, C. Wang, C. Qu, J. Liu, Y. Jin, W. Zhang and J. Jiang, *CCS Chem.*, 2021, **4**, 2588–2596.

61 H. Song, T. Y. Li, Y. Pan, X. Han, Y. Guo, L. Shi and M. Song, *Dyes Pigm.*, 2023, **219**, 111584.

62 Y. Li, N. Li, G. Li, Y. Qiao, M. Zhang, L. Zhang, Q. Guo and G. He, *J. Am. Chem. Soc.*, 2023, **145**, 9118–9128.

63 L. An, P. De La Torre, P. T. Smith, M. R. Narouz and C. J. Chang, *Angew. Chem., Int. Ed.*, 2023, **62**, e202209396.

64 F. Zhang, J. Ma, Y. Tan, G. Yu, H. Qin, L. Zheng, H. Liu and R. Li, *ACS Catal.*, 2022, **12**, 5827–5833.

65 C. Li, J. Cui, J. Zhou, Y. Xu and J. Sun, *Catal. Sci. Technol.*, 2024, **14**, 1558–1567.

66 B. Mondal and P. S. Mukherjee, *J. Am. Chem. Soc.*, 2018, **140**, 12592–12601.

67 G. Chen, W. Xin, J. Wang, J. Cheng and Y. Dong, *Chem. Commun.*, 2019, **55**, 3586–3589.

68 A. Singh, P. Verma, D. Samanta, A. Dey, J. Dey and T. K. Maji, *J. Mater. Chem. A*, 2021, **9**, 5780–5786.

69 B. Mondal, P. Bhandari and P. S. Mukherjee, *Chem.–Eur. J.*, 2020, **26**, 15007–15015.

70 H. Li, L. Geng, S. Si, H. Cheng, Z. Yang and J. Wei, *Chem. Eng. J.*, 2023, **474**, 145431.

71 Q. Fu, T. Zhang, M. An, X. Sun, Y. Li, B. Zhang, S. Zhang, G. I. N. Waterhouse, X. Liu, H. Li and S. Ai, *Chem. Eng. J.*, 2024, **492**, 152293.

72 S. Zhang, S. Wang, L. Guo, H. Chen, B. Tan and S. Jin, *J. Mater. Chem. C*, 2020, **8**, 192–200.

73 S. Fu, S. Yao, S. Guo, G. Guo, W. Yuan, T. Lu and Z. Zhang, *J. Am. Chem. Soc.*, 2021, **143**, 20792–20801.

74 L. Chen, Y. Wang, F. Yu, X. Shen and C. Duan, *J. Mater. Chem. A*, 2019, **7**, 11355–11361.

75 P. T. Smith, B. P. Benke, Z. Cao, Y. Kim, E. M. Nichols, K. Kim and C. J. Chang, *Angew. Chem., Int. Ed.*, 2018, **57**, 9684–9688.

76 X. Liu, C. Liu, X. Song, X. Ding, H. Wang, B. Yu, H. Liu, B. Han, X. Li and J. Jiang, *Chem. Sci.*, 2023, **14**, 9086–9094.

77 Y. Hu, S. Huang, L. J. Wayment, J. Wu, Q. Xu, T. Chang, Y. Chen, X. Li, B. Andi, H. Chen, Y. Jin, H. Zhu, M. Du, S. Lu and W. Zhang, *Cell Rep. Phys. Sci.*, 2023, **4**, 101285.

78 C. Chen, X. Yan, Y. Wu, S. Liu, X. Zhang, X. Sun, Q. Zhu, H. Wu and B. Han, *Angew. Chem., Int. Ed.*, 2022, **61**, e202202607.

79 L. An, M. R. Narouz, P. T. Smith, P. De La Torre and C. J. Chang, *Angew. Chem., Int. Ed.*, 2023, **62**, e202305719.

80 P. T. Smith, Y. Kim, B. P. Benke, K. Kim and C. J. Chang, *Angew. Chem., Int. Ed.*, 2020, **59**, 4902–4907.

81 P. T. Smith, B. P. Benke, L. An, Y. Kim, K. Kim and C. J. Chang, *Chemelectrochem*, 2021, **8**, 1653–1657.

82 Y. Yan, H. Qin, D. Ding, P. Yang, Q. Hou, J. Basset and Y. Chen, *Chemnanomat*, 2022, **8**, e202200305.

83 W. Wang, K. Su, E. M. El-Sayed, M. Yang and D. Yuan, *ACS Appl. Mater. Interfaces*, 2021, **13**, 24042–24050.

84 L. Feng, Y. Xie, W. Wang, K. Su and D. Yuan, *J. Mater. Chem. A*, 2023, **11**, 25316–25321.

85 Z. Wang, Y. Zhang, J. Liu, T. Wang, J. Wang, K. Yu, Y. Chen, P. Cheng and Z. Zhang, *ACS Mater. Lett.*, 2023, **5**, 2754–2759.

86 K. Su, W. Wang, S. Du, C. Ji and D. Yuan, *Nat. Commun.*, 2021, **12**, 3703.

87 Q. Zhang, H. Li, S. Chen, J. Duan and W. Jin, *J. Membr. Sci.*, 2020, **611**, 118288.

88 L. Yu, L. Hao, Y. Feng, J. Pang, M. Guo, L. Li, W. Fan, L. Fan, R. Wang, Z. Kang and D. Sun, *Nano Res.*, 2024, **17**, 4535–4543.

89 Z. Jiang, Y. Wang, M. Sheng, Z. Zha, J. Wang, Z. Wang and S. Zhao, *J. Mater. Chem. A*, 2023, **11**, 6831–6841.

90 C. Ji, K. Su, W. Wang, J. Chang, E. M. El-Sayed, L. Zhang and D. Yuan, *CCS Chem.*, 2021, **4**, 3095–3105.

91 L. Chen, P. S. Reiss, S. Y. Chong, D. Holden, K. E. Jelfs, T. Hasell, M. A. Little, A. Kewley, M. E. Briggs, A. Stephenson, K. M. Thomas, J. A. Armstrong, J. Bell, J. Busto, R. Noel, J. Liu, D. M. Strachan, P. K. Thallapally and A. I. Cooper, *Nat. Mater.*, 2014, **13**, 954–960.

92 J. M. Lucero and M. A. Carreon, *ACS Appl. Mater. Interfaces*, 2020, **12**, 32182–32188.

93 M. Liu, L. Zhang, M. A. Little, V. Kapil, M. Ceriotti, S. Yang, L. Ding, D. L. Holden, R. Balderas-Xicohténcatl, D. He, R. Clowes, S. Y. Chong, G. Schütz, L. Chen, M. Hirscher and A. I. Cooper, *Science*, 2019, **366**, 613–620.

94 D. J. Vogel, T. M. Nenoff and J. M. Rimsza, *ACS Omega*, 2022, **7**, 7963–7972.

95 T. Mitra, K. E. Jelfs, M. Schmidtmann, A. Ahmed, S. Y. Chong, D. J. Adams and A. I. Cooper, *Nat. Chem.*, 2013, **5**, 276–281.

96 A. Kewley, A. Stephenson, L. Chen, M. E. Briggs, T. Hasell and A. I. Cooper, *Chem. Mater.*, 2015, **27**, 3207–3210.

97 B. Moosa, L. O. Alimi, A. Shkurenko, A. Fakim, P. M. Bhatt, G. Zhang, M. Eddaoudi and N. M. Khashab, *Angew. Chem., Int. Ed.*, 2020, **59**, 21367–21371.

98 A. Dey, S. Chand, B. Maity, P. M. Bhatt, M. Ghosh, L. Cavallo, M. Eddaoudi and N. M. Khashab, *J. Am. Chem. Soc.*, 2021, **143**, 4090–4094.

99 Y. Ding, L. O. Alimi, B. Moosa, C. Maaliki, J. Jacquemin, F. Huang and N. M. Khashab, *Chem. Sci.*, 2021, **12**, 5315–5318.

100 Y. Ding, L. O. Alimi, J. Du, B. Hua, A. Dey, P. Yu and N. M. Khashab, *Chem. Sci.*, 2022, **13**, 3244–3248.

101 L. O. Alimi, B. Moosa, W. Lin and N. M. Khashab, *ACS Mater. Lett.*, 2024, **6**, 1467–1473.

102 A. He, Z. Jiang, Y. Wu, H. Hussain, J. Rawle, M. E. Briggs, M. A. Little, A. G. Livingston and A. I. Cooper, *Nat. Mater.*, 2022, **21**, 463–470.

103 S. Liu, J. Zhou, C. Wu, P. Zhang, X. Cao and J. Sun, *Nat. Commun.*, 2024, **15**, 2478.

104 A. Ghaffar, M. Hassan, O. V. Penkov, C. T. Yavuz and K. Celebi, *Environ. Sci. Technol.*, 2023, **57**, 20380–20391.

105 Z. Song, L. Liu, Q. Sun, J. Du, J. Guan, P. Dou, R. Zhang, Z. Jiang and J. Liu, *Angew. Chem., Int. Ed.*, 2024, **63**, e202409296.

106 L. Zhang, Y. Jia, F. Meng, L. Sun, F. Cheng, Z. Shi, R. Jiang and X. Song, *J. Alloys Compd.*, 2022, **923**, 166488.

107 Y. Xie, M. Yang, E. M. El-Sayed, K. Su, Z. Li and D. Yuan, *ACS Appl. Nano Mater.*, 2023, **6**, 7910–7919.

108 Y. Yen, T. Chen, Y. Wang, A. Robles, M. Đerić, O. Š. Miljanić, W. Kaveevivitchai and S. Chung, *J. Power Sources*, 2023, **565**, 232891.

109 R. Yan, B. Mishra, M. Traxler, J. Roeser, N. Chaoui, B. Kumbhakar, J. Schmidt, S. Li, A. Thomas and P. Pachfule, *Angew. Chem., Int. Ed.*, 2023, **62**, e202302276.

110 W. Liu, K. Wang, X. Zhan, Z. Liu, X. Yang, Y. Jin, B. Yu, L. Gong, H. Wang, D. Qi, D. Yuan and J. Jiang, *J. Am. Chem. Soc.*, 2023, **145**, 8141–8149.

111 Z. Wang, X. Wu, S. Wei, Y. Xie and C. Lu, *Chem. Mater.*, 2024, **36**, 2412–2419.

112 H. Duan, K. Li, M. Xie, J. Chen, H. Zhou, X. Wu, G. Ning, A. I. Cooper and D. Li, *J. Am. Chem. Soc.*, 2021, **143**, 19446–19453.

113 D. Cai, M. Lu, L. Li, J. Cao, D. Chen, H. Tu, J. Li and W. Han, *Small*, 2019, **15**, 1902605.

114 X. Hong, T. Tan, Y. Guo, X. Tang, J. Wang, W. Qin and Y. Cai, *Nanoscale*, 2018, **10**, 2774–2780.

115 X. Liu, X. Guo, R. Wang, Q. Liu, Z. Li, S. Zang and T. C. W. Mak, *J. Mater. Chem. A*, 2019, **7**, 2838–2844.

116 J. Zhou, R. Li, X. Fan, Y. Chen, R. Han, W. Li, J. Zheng, B. Wang and X. Li, *Energy Environ. Sci.*, 2014, **7**, 2715–2724.

117 H. Li, Y. Huang, Y. Zhang, X. Zhang, L. Zhao, W. Bao, X. Cai, K. Zhang, H. Zhao, B. Yi, L. Su, A. K. Cheetham, S. Jiang and J. Xie, *Nano Lett.*, 2022, **22**, 2030–2037.

118 A. Petronico, T. P. I. Moneypenny, B. G. Nicolau, J. S. Moore, R. G. Nuzzo and A. A. Gewirth, *J. Am. Chem. Soc.*, 2018, **140**, 7504–7509.

119 S. Bera, N. Goujon, M. Melle-Franco, D. Mecerreyes and A. Mateo-Alonso, *Chem. Sci.*, 2024, **15**, 14872–14879.

120 J. Li, J. Qi, F. Jin, F. Zhang, L. Zheng, L. Tang, R. Huang, J. Xu, H. Chen, M. Liu, Y. Qiu, A. I. Cooper, Y. Shen and L. Chen, *Nat. Commun.*, 2022, **13**, 2031.

121 Y. Xu, S. Zhang, M. Wang, Y. Meng, Z. Xie, L. Sun, C. Huang and W. Chen, *J. Am. Chem. Soc.*, 2023, **145**, 27877–27885.

122 X. Zhang, K. Su, A. G. A. Mohamed, C. Liu, Q. Sun, D. Yuan, Y. Wang, W. Xue and Y. Wang, *Energy Environ. Sci.*, 2022, **15**, 780–785.

123 F. Gao, C. Luo, X. Wang, C. Zhan, Y. Li, Y. Li, Q. Meng, M. Yang, K. Su, D. Yuan, R. Zhu and Q. Zhao, *Adv. Funct. Mater.*, 2023, **33**, 2211900.

124 Z. Yang, N. Zhang, L. Lei, C. Yu, J. Ding, P. Li, J. Chen, M. Li, S. Ling, X. Zhuang and S. Zhang, *JACS Au*, 2022, **2**, 819–826.

125 R. Han and P. Wu, *ACS Appl. Mater. Interfaces*, 2018, **10**, 18351–18358.

126 M. Liu, L. Chen, S. Lewis, S. Y. Chong, M. A. Little, T. Hasell, I. M. Aldous, C. M. Brown, M. W. Smith, C. A. Morrison, L. J. Hardwick and A. I. Cooper, *Nat. Commun.*, 2016, **7**, 12750.